JGP Journal of General Physiology

RESEARCH ARTICLE

A two-step docking site model predicting different short-term synaptic plasticity patterns

Camila Pulido and Alain Marty

The strength of synaptic transmission varies during trains of presynaptic action potentials, notably because of the depletion of synaptic vesicles available for release. It has remained unclear why some synapses display depression over time, whereas others facilitate or show a facilitation and depression sequence. Here we compare the predictions of various synaptic models assuming that several docking/release sites are acting in parallel. These models show variation of docking site occupancy during trains of action potentials due to vesicular release and site replenishment, which give rise to changes in synaptic strength. To conform with recent studies, we assume an initial docking site occupancy of <1, thus permitting site occupancy to increase during action potential trains and facilitation to occur. We consider both a standard one-step model and a more elaborate model that assumes a predocked state (two-step model). Whereas the one-step model predicts monotonic changes of synaptic strength during a train, the two-step model allows nonmonotonic changes, including the often-observed facilitation/depression sequence. Both models predict a partitioning of parameter space between initially depressing and facilitating synapses. Using data obtained from interneuron synapses in the cerebellum, we demonstrate an unusual form of depression/facilitation sequence for very high release probability after prolonged depolarization-induced transmitter release. These results indicate a depletion of predocked vesicles in the two-step model. By permitting docking site occupancy to be <1 at rest, and by incorporating a separate predocked state, we reveal that docking site models can be expanded to mimic the large variety of time-dependent changes of synaptic strength that have been observed during action potential trains. Furthermore, the two-step model provides an effective framework to identify the specific mechanisms responsible for short-term changes in synaptic strength.

Introduction

It has long been recognized that synapses tend to depress more if they release more because of the depletion of synaptic vesicles (SVs) belonging to the readily releasable pool (RRP; Betz, 1970; Zucker and Regehr, 2002). Accordingly, synapses are often classified as either depressing, when the release probability is high, or facilitating, when the release probability is low (Rozov et al., 2001; Pan and Zucker, 2009). This classification fits with the rationale that an enhanced release probability leads to a decrease of the RRP and therefore to synaptic depression (Zucker and Regehr, 2002). However, the separation between facilitating and depressing synapses is not absolute, because many synapses shift from depressing to facilitating depending on experimental conditions or display a sequence of facilitation and depression during trains of action potentials (APs). Quantitative descriptions of facilitation/depression interactions have revealed widely different patterns of synaptic plasticity in mammalian central synapses (Dittman et al., 2000). More recently, following pioneering studies at the neuromuscular junction (Betz, 1970), mechanistically rooted models incorporating variations of various synaptic vesicle pools after exocytosis, Ca^{2+}-dependent vesicle recruitment, vesicular priming, and superpriming have been developed in a few preparations (including the crayfish neuromuscular junction [Pan and Zucker, 2009], the mossy fiber–granule cell synapse [Hallermann et al., 2010], and the calyx of Held [Taschenberger et al., 2016]). These studies have stressed the necessity to correct for synaptic jitter and for changes in quantal size caused by receptor saturation and desensitization when linking excitatory postsynaptic current amplitudes to release models (Taschenberger et al., 2005; Hallermann et al., 2010). Because of these limitations and persisting uncertainties on vesicular pool dynamics (Pan and Zucker, 2009), the link between release probability and short-term synaptic plasticity has remained qualitative in many central synapses, mostly relating the

Laboratory of Brain Physiology, Centre National de la Recherche Scientifique Unité Mixte de Recherche 8118, Paris Descartes University, Paris, France.

Correspondence to Alain Marty: alain.marty@parisdescartes.fr; C. Pulido's present address is Dept. of Biochemistry, Weill Cornell Medical College, New York, NY.

directions of changes for the initial release probability and for the paired-pulse ratio (PPR).

In recent years, SV release has been modeled supposing a finite number of presynaptic structures called docking sites or release sites, where each docking site maximally releases one SV in response to a presynaptic AP. The docking site hypothesis can be traced back to Katz (1969) and has received extensive support from subsequent genetic, morphological, and functional studies (Südhof, 2012). If the synapse is stimulated by an AP train, docking site occupancy by an SV may be modeled as a Markov chain. In the simplest version of such models, called one-step model hereafter, docking site occupancy is governed by two simple kinetic processes (Quastel, 1997; Scheuss and Neher, 2001). On one hand, when an AP arrives, a docked SV has a probability (p) to be released. On the other hand, once a docking site is empty, docking site replenishment results from a transition from an infinite pool of recycling SVs, yielding a probability of recovery (r) during one interstimulus interval. Markov chain models of docking sites potentially provide a rigorous basis for the interpretation of short-term synaptic plasticity, but this approach remains underexploited (Pulido and Marty, 2017). Based on the one-step model, it is possible to account for the decay of excitatory postsynaptic current amplitudes in depressing synapses (Rozov et al., 2001; Hallermann et al., 2010). However, one-step models have until very recently assumed that the initial docking site occupancy is 1, whereas more recent data indicate that this is not generally the case (Trigo et al., 2012; Pulido et al., 2015; Miki et al., 2016). Assuming incomplete initial docking site occupancy opens new perspectives to model short-term synaptic plasticity, the present work takes advantage of this possibility.

Another limitation of existing release/docking site models of synaptic plasticity is that they focus almost exclusively on the one-step docking model. However, several recent studies suggest that the one-step model is an oversimplified representation of synaptic function. In particular, it has been suggested that two types of release sites may be involved in some synapses, either independent of each other or coupled together (Neher and Sakaba, 2008; Hallermann et al., 2010; Lee et al., 2012; Neher, 2017). Based on an analysis of cumulative counts of SV release during AP trains in synapses between cerebellar parallel fibers and molecular layer interneurons (MLIs), a two-step model has been proposed where SVs transit through a replacement site before binding to the docking site (Miki et al., 2016). The two-step model offers the possibility to account for a facilitation/depression sequence even if *p* does not change during the train (Pan and Zucker, 2009; Miki et al., 2016). In the present work, we examine the patterns of short-term synaptic plasticity that are displayed by one-step and two-step models, incorporating the possibility that the resting docking site occupancy may be <1. We illustrate the applicability of this approach by investigating, at synapses between cerebellar MLIs, a form of synaptic modification that is induced by changes in the presynaptic holding potential (Bouhours et al., 2011; Christie et al., 2011). The results show that depolarization induces an unusual depression/facilitation sequence that can be explained more readily by the two-step model than by the one-step model. Within the two-step model, the results further indicate which kinetic steps are preferentially altered by presynaptic depolarization. Our work highlights the versatility of short-term synaptic plasticity patterns associated with the two-step docking site model, and it offers a widely applicable approach to identify cellular mechanisms underlying synaptic changes.

Materials and methods

Recording procedures

Sagittal slices (200 µm thick) were prepared from the cerebellar vermis of Sprague-Dawley rats (postnatal 12–14) following the animal care guidelines of our host institution (Université Paris Descartes; approval number A-750607). Procedures to record from MLIs were as described (Llano and Gerschenfeld, 1993). The composition of the standard extracellular solution was (in mM) 130 NaCl, 2.5 KCl, 26 $NaHCO_3$, 1.3 NaH_2PO_4, 10 glucose, 2 $CaCl_2$, and 1 $MgCl_2$ (300 mosmol/liter). This solution was equilibrated with 95% O_2 and 5% CO_2, pH 7.4. The standard internal recording solution contained (in mM) 145 KCl, 4.6 $MgCl_2$, 2 EGTA, 10 HEPES-K, 0.4 NaGTP, 4 Na_2ATP, and 10 gamma-aminobutyric acid (GABA), pH 7.4 (300 mosmol). GABA was included in this solution to prevent emptying of the synaptic vesicles and consequent postsynaptic current (PSC) rundown (Bouhours et al., 2011). All recordings were at room temperature.

Paired MLI recordings

Dual whole-cell recordings were obtained from neighboring MLIs using a triple EPC-10 amplifier (Heka). The probability to obtain synaptically connected pairs was on the order of 10%. According to previous work, a connection was considered to involve a simple synapse if the PSC amplitude histogram displayed a single Gaussian peak with a coefficient of variation value <0.35 (Kondo and Marty, 1998). Both pre- and postsynaptic MLIs were maintained in voltage clamp; the holding potential of the postsynaptic cell was maintained at −60 mV, whereas the holding potential of the presynaptic cell was varied between −80, −60, and −50 mV. PSCs were elicited by presynaptic voltage steps to 0 mV (1-ms duration). Trains of 5 or 10 such pulses (40- or 20-ms interstimulus intervals, respectively) were applied repetitively, with intervals of 10 s between trains. Part of the experimental dataset was common with that of a recent publication (Pulido et al., 2015) and was reanalyzed.

Modeling vesicular release at an individual docking site

In a docking site model, the release probability $P_D(S_i)$ in response to the ith stimulation in an AP train is the product of the probability that the docking site is occupied, δ_i, with the release probability of a docked SV, p (Scheuss and Neher, 2001):

$$P_D(S_i) = \delta_i p. \quad (1)$$

Here we examine the evolution of the release probability $P_D(S_i)$ as a function of i in two different docking site models. For simplicity, we assume that docking sites are independent of each other and that they all have identical release parameters. In addition, we assume that p is independent of i. This last assumption is consistent with measurements of calcium entry in single MLI varicosities using two-photon microscopy, showing identical calcium entries for successive APs (Pulido et al., 2015). Note, however, that

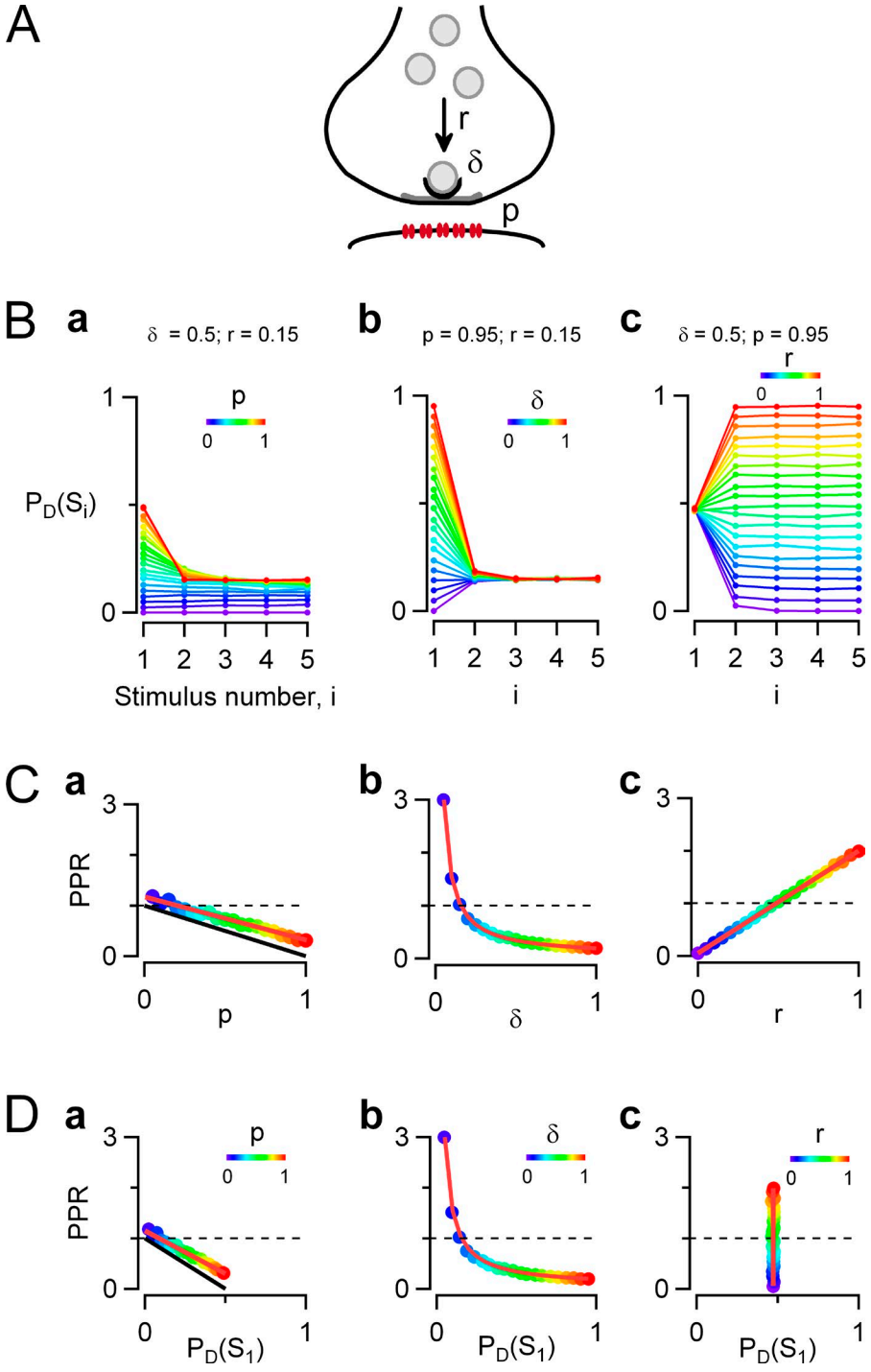

Figure 1. **Simple docking site model of release probability during train stimulation.** Monte Carlo simulations were performed to predict the evolution of the vesicular release probability ($P_D[S_i]$) at one docking site during AP trains, as a function of stimulation number, i. **(A)** Schematic representation of one-step release model on a synapse with a single active zone (gray) and associated postsynaptic receptors (red). Synaptic vesicles (light gray) are recruited from an infinite reserve pool, and just one is bound to a docking site (black) before exocytosis. Here a single docking site is represented, but in reality, simple synapses contain variable docking site numbers, on a range varying from 1 to 6 for MLI–MLI synapses. Reference values for the parameters of the model are similar to values previously obtained at MLI–MLI synapses (Pulido et al., 2015): the docking site occupancy is δ = 0.5 before the train stimulation; the probability of release of a docked vesicle in response to an AP is p = 0.95; and after release, an emptied docking site is replenished from an infinite vesicle pool with a fixed transition probability r = 0.15, estimated over one interstimulus interval (stimulation frequency is 25 Hz). **(B)** The evolution of $P_D(S_i)$ as a function of i was examined when synaptic parameters p, δ, and r were separately incremented from 0 to 1 (color code is violet to red, with 0.05 increments for each parameter). **(C)** PPR plots as a function of each of the three synaptic parameters show that PPR values follow a decreasing linear dependence on p and a decreasing hyperbolic dependence on δ and follow an increasing linear dependence on r (color-coded dots, simulations; red traces, model predictions from Eq. 5). Changing any of the three parameters p, δ, or r allows shifting from a depressing synapse (PPR < 1) to a potentiating synapse (PPR > 1; PPR = 1 indicated by dotted lines). **(D)** PPR as a function of $P_D(S_1)$ in the three conditions where each synaptic parameter is modified. In B–D, modified parameters are (a) p (with predictions for the special case where r is very small shown in black), (b) δ, and (c) r. In each case, the remaining parameters are kept at their reference values.

the possibility remains that p could be altered by another mechanism such as saturation of a fast calcium buffer (Rozov et al., 2001). For i = 1 we note $\delta_1 = \delta$. During a train, δ_i varies, and $P_D(S_i)$ follows δ_i changes proportionally according to Eq. 1. We note

$$PPR = P_D(S_2)/P_D(S_1).$$

In view of Eq. 1, this can be rewritten as

$$PPR = \delta_2/\delta. \quad (2)$$

In the simple docking site model illustrated in Fig. 1 A, docking site replenishment appears as a single transition reflecting the transfer of one vesicle from the reserve pool to an empty docking site. This transition occurs with a fixed rate constant R, so that the probability of transition during an interval Δt is $r = 1 - \exp(-R\Delta t)$. In the simulations of Fig. 1 A, Δt was chosen as 40 ms. In line with previous work (Pulido et al., 2015), the reference value for r was 0.15, reflecting a probability of refilling of an empty docking site of 0.15 over a period of 40 ms.

The relation between δ_{i+1} and δ_i (the probability that the docking sites are occupied before stimulus [i + 1] and i, respectively) can be derived from the laws of conditional probabilities (Scheuss and Neher, 2001; Pulido et al., 2015) as

$$\delta_{i+1} = \delta_i(1 - p) + \delta_i pr + (1 - \delta_i)r. \quad (3)$$

Making i = 1 in the above equation leads to

$$\delta_2 = \delta(1 - p) + \delta pr + (1 - \delta)r. \quad (4)$$

Combining Eqs. 2 and 4 gives

$$PPR = (1 - p) + pr + (1/\delta - 1)r. \quad (5)$$

This equation was used to produce the theoretical curves shown in red in Fig. 1 C, a–c. It predicts a linear dependence of PPR on p (Fig. 1 C, a) and on r (Fig. 1 C, c) and a hyperbolic dependence of PPR on δ (Fig. 1 C, b). These curves are in good agreement with corresponding Monte Carlo simulations (dots; see next section).

Eq. 3 allows one to calculate δ_i for all i values by iteration, leading to the calculation of $P_D(S_i)$ curves as in Fig. 1 B by using Eq. 1. It can be verified that $P_D(S_i)$ curves are always monotonic with the model of Fig. 1 A. This is because the underlying Markov process has two states (the docking site being either empty or occupied; Scheuss and Neher, 2001) and relaxes from its initial state to steady state following a monotonic exponential time course.

Applying Eq. 1 to the case i = 1 indicates that the initial release probability is

$$P_D(S_1) = \delta p. \quad (6)$$

Therefore, if either p or δ is changed while keeping the other parameter constant, PPR versus $P_D(S_i)$ plots can be obtained from the PPR versus p and PPR versus δ plots by appropriate scaling of the abscissa (Fig. 1 D, b; compare with Fig. 1 C, a and b).

Eq. 5 takes simpler forms in two practically important limiting cases. If all docking sites are occupied at rest (δ = 1), it reduces to

$$PPR = 1 - p + pr. \quad (7)$$

Because both p and r are comprised between 0 and 1, Eq. 7 predicts that for δ = 1, the synapse is depressing (PPR < 1). Accordingly, the left front face of the parameter cube in Fig. 2 representing the case δ = 1 is entirely in the depressing region. The other limiting case is obtained by making r = 0 in Eq. 5, as occurs at very high stimulation frequency. Eq. 5 then reduces to the previously derived relation (Betz, 1970; Rozov et al., 2001; Taschenberger et al., 2005; Lu and Trussell, 2016)

$$PPR = 1 - p. \quad (8)$$

Eq. 8 was used to predict the black lines in Fig. 1 C, a, and in Fig. 1 D.

Markov chain representation of one-step and two-step docking models

Fig. 4 A shows a Markov chain representation of the one-step model (Quastel, 1997). One docking site can switch from vacant (Fig. 4 A, left) to occupied (Fig. 4 A, right), with a forward rate constant R and a backward rate constant P. We assume that R remains constant within an AP train, as mentioned earlier. However, P is time dependent and takes a nonzero value only during a short time after each AP, so that p is the integral of P(t) over the period Δt. With these assumptions, $P_D(S_i)$ follows an exponential time course as a function of i and therefore is a monotonic function of i (either continuously increasing throughout the train or continuously decreasing throughout the train).

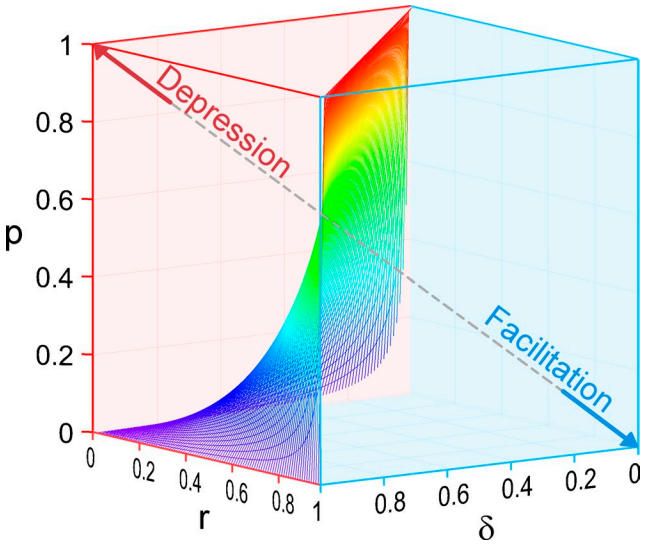

Figure 2. **Partitioning of parameter space between depressing and facilitating synapses.** The parameter space describing the one-step docking model is represented by a cube where all three parameters p, δ, and r vary from 0 to 1. The axis origin (coordinates 0, 0, 0) is located at the bottom rear corner of this cube. Facilitating synapses appear on the right in this representation (blue space, with a facilitation pole at p = 0, δ = 0, r = 1), and depressing synapses appear on the left (red space, with a depression pole at p = 1, δ = 1, r = 0). The partition between the two regions is a curved surface defined by the relation p = (1/δ − 1)r/(1 − r).

Fig. 4 B shows a Markov chain representation of the two-step model. As in the one-step model, P is the release rate of docked SVs, and the integral of P over the interval Δt is p. In the two-step model, docking site replenishment is a two-step process involving a replacement site associated to the docking site, in accordance with a recently developed model (Miki et al., 2016). In this model, the replacement site is filled from an infinite reserve pool with a rate constant S. Once the replacement site is occupied, the transition from the replacement site to the docking site follows a simple step with rate constant R′. As before, transition rate constants S and R′ are assumed constant throughout the AP train for simplicity. They are then related to corresponding transition probabilities during one interstimulus interval by the relations s = 1 − exp(−SΔt) and r′ = 1 − exp(−R′Δt).

Although the one-step model predicts a monotonic time course of $P_D(S_i)$, more complex time courses are predicted by the two-step model, as shown in Fig. 3. Because of the complexity of the two-step model, analytical solutions are awkward to handle, and Monte Carlo simulations were performed instead with time increments of 4 ms for 25-Hz data and 2 ms for 50-Hz data (10 time increments per interstimulus interval in each case). For each set of parameter values, 5,000 simulations were performed, and their results were averaged together.

In the two-step model, Eqs. 1 and 2 are still valid, but Eqs. 3, 4, and 5 need to be qualified. The rate of replenishment of empty docking sites is not constant, because the probability of occupancy of the replacement site is time dependent. Therefore, for each value of i, r needs to be calculated by solving the evolution of ρ as a function of time during the time interval that is considered.

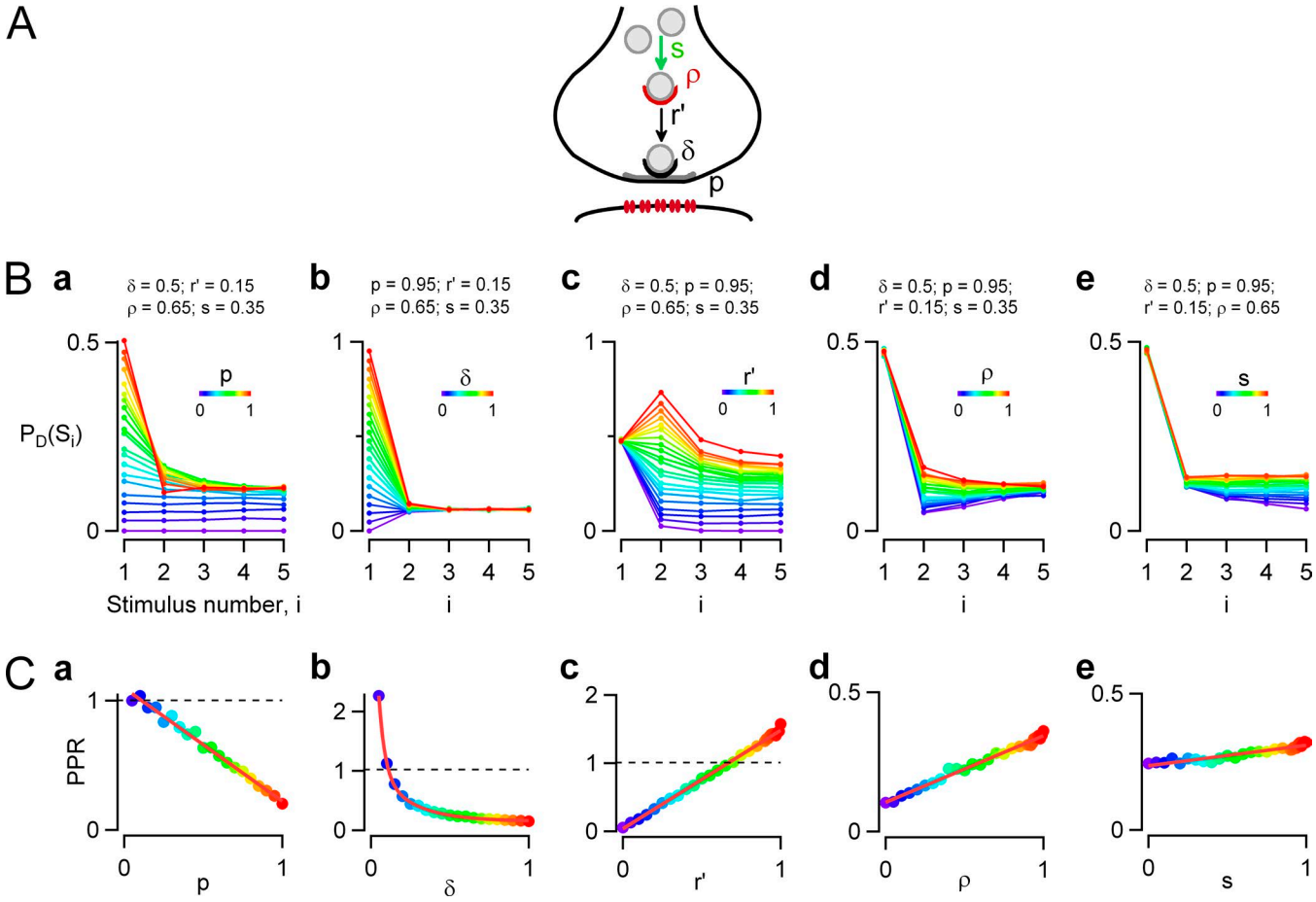

Figure 3. **Two-step docking site model.** Monte Carlo simulations were performed to predict synaptic responses to an AP train in a two-step docking model, depending on each kinetic parameter of the model. **(A)** Scheme describing the two-step model, where a replacement site (red) is associated to each docking site (gray). The replacement site can be either empty or occupied by an SV and has an initial probability of occupancy ρ before a train. If it is empty, it cannot replenish the associated docking site in case of release. If it is occupied, it can supply an SV to the depleted docking site, with a probability of recovery r′ during one interspike interval. Emptied replacement sites are replenished from an infinite SV pool with a transition probability s, again applying for one interspike interval. **(B)** Simulations examining the evolution of $P_D(S_i)$ as a function of i when each one of the five synaptic parameters is separately incremented from 0 to 1 (color code is violet to red). The other four parameters are kept at reference values (indicated above each plot) mimicking control conditions for MLI–MLI synapses. **(C)** PPR analysis as a function of individual synaptic parameters. Linear relations are obtained when any of the parameters p (a), r′ (c), ρ (d), or s (e) is examined; in the case of δ (b), the relation is hyperbolic (color-coded dots, simulations; red, regression lines). Reference parameter values are p = 0.95, δ = 0.5, r′ = 0.15, ρ = 0.65, and s = 0.35 and refer to MLI–MLI synapses.

This leads to a series of r_i values that differ depending on i. r_i is a complicated function of ρ_i, r′, and s:

$$r_i = \rho_i r' - (1-\rho_i)\ln(1-r')\ln(1-s) \times \{1-[1-(1-r')(1-s)]/[\ln(1-r')+\ln(1-s)]\} \div [\ln(1-r')+\ln(1-s)]. \quad (9)$$

In this equation, r_i represents the probability of replenishment of empty docking sites during the interval between AP number i and AP number (i + 1), and ρ_i represents the probability of occupancy of the replacement site just before AP number i. Eq. 3 remains valid provided that r is replaced by r_i. In Eqs. 4 and 5, r should be replaced by r_1 as i = 1. Eq. 9 shows that r_i is a linear function of ρ_i. In particular for i = 1, entering $\rho_1 = \rho$ in Eq. 9 yields

$$r_1 = \rho r' - (1-\rho)\ln(1-r')\ln(1-s) \times \{1-[1-(1-r')(1-s)]/[\ln(1-r')+\ln(1-s)]\} \div [\ln(1-r')+\ln(1-s)]. \quad (10)$$

Eq. 10 shows that r_1 is a linear function of ρ. Therefore, in view of Eq. 5, the PPR is a linear function of ρ, as illustrated in Fig. 3 C, d. Concerning r′ and s, the relations are not exactly linear but are nevertheless well approximated by linear functions for the parameter values examined here (Fig. 3 C, c and e).

Relating synaptic release statistics and docking site models

In general, synaptic connections among MLIs involve more than one docking site. To estimate the number N of docking sites implicated in one paired recording experiment, we followed the method of Pulido et al. (2015). This method first assumes that the RRP size applying before the first pulse is fixed, with a value n = δN. Second, it neglects the recovery rate so that r = 0. In view of the first assumption the failure probability after the first pulse is

$$P(F_1) = (1-p)^n. \quad (11)$$

After the first pulse, the RRP size drops from the initial value n to the new value n(1 − p). Under the second assumption that r = 0, we have

$$P(F_2) = (1-p)^{n(1-p)}. \quad (12)$$

Combining Eqs. 11 and 12 yields

$$n = \log[P(F_1)]/\log\{\log[P(F_2)]/\log[P(F_1)]\}. \quad (13)$$

To obtain N, we take the integral number closest to the ratio between the value of n derived from Eq. 13 and the value of δ, taken as 0.5 (Pulido et al., 2015).

For N independent and equivalent docking sites, the probability of failure in response to the ith stimulation at the level of the synapse, $P(F_j)$, is related to the probability of failure at the level of one docking site, $P_D(F_j)$, by

$$P(F_j) = P_D(F_j)^N.$$

Corresponding success probabilities are therefore related to each other by

$$P(S_j) = 1 - P(F_j) = 1 - [1 - P_D(S_j)]^N$$

so that

$$P_D(S_j) = 1 - [1 - P(S_j)]^{1/N}. \quad (14)$$

Once the value of N was determined using Eq. 13, $P_D(S_j)$ was derived from the measurements of $P(S_j)$ according to Eq. 14.

To obtain the parameter values in the 25-Hz simulations of Fig. 7, each of the five parameters p, δ, r′, ρ, and s was incremented in steps of 0.05 between 0 and 1, and best values were determined using minimal sums of least square deviations from the mean data. Once a set of parameters was obtained for 25 Hz, it was also used to model 50-Hz data as explained in Results.

Results

Short-term synaptic plasticity in a one-step docking site model

In this work, we relate the evolution of released SV numbers during an AP train with specific models of docking site function, using MLI–MLI synapses as reference. Previous work has shown that many MLI–MLI synapses have a single presynaptic active zone and a single postsynaptic density of GABA receptors; such synapses are called simple synapses (Auger et al., 1998; Kondo and Marty, 1998). Release statistics suggest that simple synapses have variable numbers of docking sites (N, in the range 1–6; Trigo et al., 2012; Pulido et al., 2015), where SV release can as a first approximation be described by the one-step model of Fig. 1 A (Quastel, 1997; Scheuss and Neher, 2001). This model is characterized by three parameters: p, r, and δ, where p is the release probability of an occupied docking site in response to an AP, δ is the occupancy of the docking site at rest, and r is the probability of replenishment of empty docking sites from an infinite reservoir, calculated over one interstimulus interval (Fig. 1 A). The release probability of one docking site in response to the ith AP of a train, $P_D(S_i)$, can be estimated by multiplying the probability of release of a docked SV (p) together with the probability δ_i that the docking site is occupied by an SV (Eq. 1). In this work we assume that p is constant throughout an AP train, in agreement with previous results and interpretations (Pulido et al., 2015). δ_i can be calculated by an iterative method derived from Eqs. 1 and 3. Because the number of docking sites is merely a scaling factor, δ_i indicates the evolution of synaptic strength during an AP train. We take as reference the following parameter values, based on our previous analysis of mean data (Pulido et al., 2015) as well as on new simulations to be presented below: p = 0.95, r = 0.15, and δ = 0.5. In this model, the probability of exocytosis of docked vesicles is very high, yet the probability of release in response to the first AP is <0.5 ($P_D[S_1] = 0.95 \times 0.5 = 0.475$) because the resting docking site occupancy is only 0.5. With these values the synapse is depressing, and $P_D(S_i)$ stabilizes slightly below 0.2 for i > 2 (Fig. 1 B, a, orange curve). The PPR can be calculated using Eq. 5, giving PPR = 0.342.

Effects of changing individual parameter values within the one-step model on short-term synaptic plasticity

The simulations displayed in Fig. 1 B, a–c, illustrate how $P_D(S_i)$ plots are modified when each of the three parameters p, δ, or r is altered, keeping the other two parameters constant. In all cases, the one-step docking site model predicts a monotonic change of $P_D(S_i)$ with i. High values of p or δ lead to depression (Fig. 1 B, a and b, hot colors: red, yellow, and green tones), whereas low δ values lead to facilitation (Fig. 1 B, b, cold colors: violet, blue, and cyan tones). Conversely, high values of r lead to facilitation, whereas low values of r lead to depression (Fig. 1 B, c). Therefore, depending on the values of p, δ, and r, the synapse is either depressing or facilitating, and it remains so throughout the stimulation train.

A quantitative assessment of the extent of facilitation or depression is shown in Fig. 1 C, where the PPR is plotted as a function of each of the altered parameters. If p is altered between 0 and 1, keeping both r and δ at reference values, Eq. 5 predicts a linear dependence of the PPR on p (Fig. 1 C, a, colored dots and superimposed red line). If p is close to 0, $P_D(S_1)$ is very small, and the synapse is potentiating (making p = 0 in Eq. 5 leads to PPR = 1 + r [1/δ − 1] = 1.15). At the other extreme, if p = 1, $P_D(S_1)$ reaches its maximum ($P_D[S_1] = \delta = 0.5$), and the PPR takes its minimal value (PPR = r/δ = 0.30). The results of Fig. 1 C, a, confirm not only the well-known rule that as p increases, the PPR decreases after SV depletion (Betz, 1970), but also that the relation between PPR and p is linear (Betz, 1970). In the limit of very high stimulation frequency (r = 0), the relation PPR = 1 − p is predicted (Eq. 8 and Fig. 1 C, a, black line). For other r values the PPR versus p line lies above this limiting case, as exemplified in Fig. 1 C, a, for the reference value r = 0.15.

As δ is changed between 0 and 1, the synapse changes from potentiating (with a PPR value that becomes infinite for δ = 0) to depressing (with PPR = 1 − p[1 − r] = 0.192 if δ = 1), following a hyperbolic curve (Fig. 1 C, b).

Finally, Fig. 1 C, c, shows that as r is changed, the synapse shifts from depressing (with PPR = 1 − p = 0.05 at r = 0) to potentiating (with RRP = 1/δ = 2.0 for r = 1), following a linear relation.

In Fig. 1 D, the PPR is plotted as a function of the initial release probability per docking site $P_D(S_1)$. Plotting PPR in this manner is of interest because $P_D(S_1)$ is proportional to synaptic strength, which can be evaluated experimentally. The relation is either

linear or hyperbolic, depending on whether changes in $P_D(S_1)$ result from alterations of p (Fig. 1 D) or δ (Fig. 1 D, b). When r is modified, $P_D(S_1)$ is not changed, yet large changes of the PPR are obtained (Fig. 1 D, c). Thus, the one-step model does not predict an obligatory relation between PPR and $P_D(S_1)$. Rather, specific changes in the synaptic parameters p, δ, and r yield different patterns of concerted changes in PPR and $P_D(S_1)$.

Parameter domains corresponding to facilitating and depressing synapses

The simulations of Fig. 1 show that a synapse can shift from facilitating (PPR > 1) to depressing (PPR < 1) by changing any of the three parameters p, δ, and r. A limitation of this result is that it was obtained using characteristic parameter values of MLI–MLI synapses as reference. To overcome this restriction, we next aimed to extend the conclusions of Fig. 1 to an arbitrary set of initial parameter values. In general, the transition between facilitation and depression can be obtained by making PPR = 1 in Eq. 5, leading to the result

$$p = (1/\delta - 1)r/(1 - r).$$

Parameter sets that verify the above equation define a curved surface in the cubic parameter space obtained by varying values of p, δ, and r between 0 and 1 (Fig. 2). In Fig. 2, synapses are depressing in the portion of the cube located on the left of this surface, whereas they are facilitating in the portion located on the right of the surface. Two poles are located at opposite corners of the parameter space, a depression pole corresponding to p = 1, δ = 1, r = 0 (Fig. 2, red arrow), and a facilitation pole corresponding to p = 0, δ = 0, r = 1 (Fig. 2, blue arrow).

Of the six faces of the cube shown in Fig. 2, five are entirely located either in the facilitation space (three faces in blue) or in the depression space (two faces in red). Both the r = 0 face (corresponding to very high stimulation frequency) and the δ = 1 face (total initial docking site occupancy) predict depression. In contrast, the p = 0, δ = 0, and r = 1 faces all predict facilitation. The sixth face, with p = 1, is divided between a depressing area, where r < δ, and a facilitating area, where r > δ. These results are in accord with the common observations that at high enough frequency, synapses tend to become depressing, and that at low enough release probability, all synapses are facilitating.

In conclusion, according to the one-step model, all three parameters p, δ, and r are equally important in controlling the nature of short-term synaptic plasticity. Facilitation and depression each occupy a certain parameter domain, and synapses can shift from one status to the other by crossing the boundary surface depicted in Fig. 2.

Short-term synaptic plasticity in a two-step docking site model

The model of Fig. 1 may be too simple. Although some central synapses display monotonic PSC amplitude increases or decreases during trains (Rozov et al., 2001), in many other central synapses a facilitating/depressing sequence is observed (Taschenberger et al., 2005; Bao et al., 2010) as previously described in the frog neuromuscular junction (Del Castillo and Katz, 1954) or at the squid giant synapse (Charlton et al., 1982). Because under our assumptions (constant p and r values) such patterns cannot be explained with the one-step model of Fig. 1, we next explored whether they could result from more complicated docking models. Analysis of vesicular release statistics at simple synapses (both at parallel fiber–MLI synapses and at MLI–MLI synapses) has led to the suggestion that each docking site is associated with another site, called a replacement site (Miki et al., 2016; Fig. 3 A). The replacement site is either empty or occupied with an occupancy probability called ρ. If the replacement site is occupied, and if the docking site is free, the transition from replacement site to docking site has a probability r′ (similar to the parameter r of the previous model); however, if the replacement site is empty, the probability of replacement at the docking site drops to 0. Likewise, if the docking site is occupied, the transition r′ is blocked. The supply of the replacement site from reserve SVs occurs with a probability s, provided that the replacement site is empty. We next investigated short-term synaptic plasticity in this more elaborate model, called the two-step model. We took as reference values a series of parameters that mimic the properties of MLI–MLI synapses: p = 0.95, δ = 0.5, r′ = 0.15, ρ = 0.65, and s = 0.35 (see simulations in Fig. 7). Like before, we examined the changes in $P_D(S_i)$ patterns when altering each parameter around these reference values.

Effects of changing individual parameter values within the two-step model on short-term synaptic plasticity

A comparison between Figs. 1 and 3 reveals a striking difference between one-step and two-step models: whereas the synaptic response varies monotonically during an AP train in the one-step model, this response can go through a maximum or through a minimum in the two-step model. As detailed in Materials and methods, this difference arises because the Markov chain representing the one-step model is a single equilibrium exchange, whereas that representing the two-step model contains several interlinked equilibria. In the two-step model, both facilitating–depressing sequences (Fig. 3 B, c, red curves) and depressing–facilitating sequences (Fig. 3 B, d, blue curves) are obtained alongside monotonic responses (Fig. 3 B, c, blue curves, and Fig. 3 B, d, red curves).

As shown in Fig. 3 B, a and b, and Fig. 3 C, a and b, changing either p or δ produced changes in $P_D(S_i)$ and PPR that were roughly similar to those obtained earlier with the one-step model. Fig. 3 B, c–e, examines the effects of changing r′, ρ, and s, which collectively are responsible for docking site replenishment. Because these parameters do not influence $P_D(S_1)$, all curves in Fig. 3 B, c–e, start from a common $P_D(S_1)$ value. Nevertheless, differences in $P_D(S_i)$ plots appear later in the train. Fig. 3 B, c, illustrates wide variations in $P_D(S_i)$ curves depending on r′. At low values (Fig. 3 B, c, violet/blue curves), the response remains depressing throughout the train, but at high r′ values a facilitating/depressing pattern is observed (Fig. 3 B, c, yellow/red curves). Variations of $P_D(S_i)$ as a function of ρ are comparatively simpler (Fig. 3 B, d). Starting with identical $P_D(S_1)$ values, the responses diverge for i = 2 depending on ρ, but they converge at the end of the train to similar steady-state values. As a result, responses exhibit a marked depressing/facilitating sequence for low ρ values (Fig. 3 B, d, violet/blue curves), and they decrease

monotonically for large ρ values (Fig. 3 B, d, hot colors). Finally, Fig. 3 B, e, examines the effects of changing s. The responses gradually diverge from each other as i increases. For very low s values the responses are monotonically depressing; however, at higher s values the responses are essentially stable for i > 1 (Fig. 3 B, e, green/yellow/red curves).

In Fig. 3 C, we plotted the changes of the PPR as a function of the five parameters: p, δ, r′, ρ, and s. As in the one-step model, the PPR had a linear dependence on p (Fig. 3 C, a) and a hyperbolic dependence on δ (Fig. 3 C, b). In addition, according to Eq. 10, the PPR varied linearly with ρ and almost linearly with r′ and s (Fig. 3 C, c–e; Materials and methods).

Next, we asked whether the partitioning of parameter space shown in Fig. 2 for the one-step model can be extended to the two-step model. Because the two-step model has five free parameters it cannot be represented fully in a single tridimensional plot. In addition, whereas responses vary monotonically in the one-step model, biphasic profiles (facilitating/depressing, as well as depressing/facilitating) can occur in the two-step model, as discussed next. In spite of these complications, Fig. 2 can still be used within the framework of the two-step model to predict whether the response is initially facilitating or depressing, by calculating r from s, r′, and ρ according to Eq. 10 and by using that r value together with the relevant p and δ values in the tridimensional plot of Fig. 2. An important result that is common for both one-step and two-step models is that if δ = 1, the synapse is initially depressing: this corresponds to the face of the parameter cube that is located on the left and in the front of the representation of Fig. 2. Conversely, if either δ or p is close to 0 (leading in each case to $P_D[S_1] \sim 0$ according to Eq. 6), the synapse is initially facilitating (Fig. 2, blue right face and bottom face). If r = 1, because of very efficient and complete docking, the synapse is initially facilitating (Fig. 2, blue front face of the cube). Finally, if r is close to 0, as occurs at very high frequency, the synapse is initially depressing (Fig. 2, rear left face of the cube).

In summary, the three-dimensional plot of Fig. 2 gives a representation of the initial trend of short-term synaptic plasticity (depressing or facilitating) that applies both for the one-step model and for the two-step model.

The time course of synaptic strength changes during trains is monotonic in the one-step model but can be biphasic in the two-step model

A key advantage of release/docking site models is that they can be interpreted as a series of interconnected states forming a Markov chain (Quastel, 1997; Scheuss and Neher, 2001; Pulido and Marty, 2017). Whereas the one-step model can be described with a single kinetic exchange between two states, making a very simple Markov chain (Fig. 4 A), the two-step model involves four distinct states (Fig. 4 B). Accordingly, in the one-step model of Fig. 1, $P_D(S_i)$ curves are monotonic, but more complex patterns appear with the two-step model (Materials and methods). For certain parameter combinations the familiar facilitation/depression sequence is obtained (e.g., Fig. 3 B, c, red curves). This pattern arises if early in the train ρ is elevated, so that docking site replenishment exceeds docking site depletion after release, whereas later in the train ρ is low, so that docking site replenishment does not offset

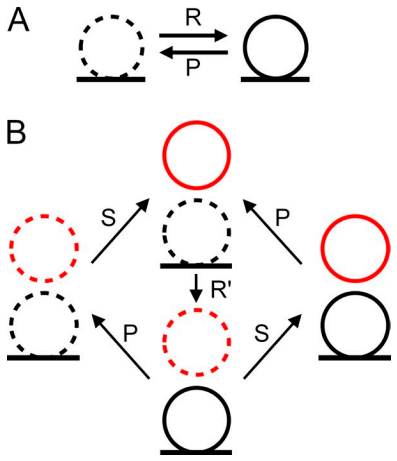

Figure 4. **Markov chain representations of the one-step and two-step models. (A)** One-step model. The docking site is either empty (left, dotted SV) or occupied (right, continuous SV), and transitions between the two states occur with forward rate R and backward rate P. Transition probabilities r and p during an inter-AP interval Δt are related to R and P as explained in Materials and methods. **(B)** Two-step model. Here four different states occur, depending of the occupancy of the docking site (bottom, black) and of its associated replacement site (top, red; in this representation, δ is the summed probability of states with continuous black SVs, and ρ is the summed probability of states with continuous red SVs). States are linked with transition rates as indicated. Transition probabilities r' (docking) and s (replenishment from reserve pool) are related to rate constants R' and S as explained in Materials and methods. All transitions are assumed unidirectional for simplicity, but a more general model would include backward rates for each transition.

docking site depletion after release. By this mechanism a slow fall in ρ induces an initial rise followed by a fall in δ. Such a gradual fall in ρ values is favored by higher values of r′ and ρ and lower values of s (Fig. 3 B, c, and simulations not depicted). It occurs under standard experimental conditions in a large number of preparations, including the frog neuromuscular junction (Del Castillo and Katz, 1954). In the mammalian brain, it is notably observed in many glutamatergic synapses including the calyx of Held (Taschenberger et al., 2005; Sakaba, 2006) and PF–MLI synapses (Bao et al., 2010; Ishiyama et al., 2014). Strikingly, the opposite depression/potentiation sequence also appears in our simulations (Fig. 3 B, d, blue curves). This case appeared particularly interesting to us because whereas examples of synapses exhibiting a facilitating/depressing sequence are widespread, previous studies of a depressing/facilitating sequence are very scarce. In fact, we are aware of a single such study, in a study of the human neuromuscular junction by Elmqvist and Quastel (1965). Under control conditions, the facilitating/depressing sequence was sporadically observed in this study at high frequency with preparations exhibiting marked synaptic depression. The depressing/facilitating sequence was more reliably obtained after a potentiating tetanus train, particularly in elevated extracellular Ca^{2+} conditions (8 mM). These results indicate that the depressing/facilitating sequence is favored by very high release probability (Elmqvist and Quastel, 1965).

To explain the striking contrast between the scarcity of experimental studies of the depression/facilitation sequence and the plethora of examples of the opposite facilitation/depression sequence, we next aimed to identify the exact conditions leading

to the depression/facilitation sequence in the two-step model and to define experimental manipulations that would reliably lead to this sequence. Beyond the immediate goal of understanding the conditions of the depression/facilitation sequence, solving this issue appears as a challenging test of the relevance of the docking site models to explain short-term synaptic plasticity.

Presynaptic depolarization induces a depressing/facilitating sequence at MLI–MLI synapses

Several lines of evidence indicate that MLI–MLI synapses display a high release probability. Release of GABA from MLI axons is little affected by the slow calcium buffer EGTA, as measured either in MLI–Purkinje cell synapses (Arai and Jonas, 2014) or in MLI autoreceptor currents (Bouhours et al., 2011), whereas the fast calcium buffer BAPTA is much more effective (Pouzat and Marty, 1999; Arai and Jonas, 2014). These results indicate close coupling between presynaptic calcium channels and SVs and are suggestive of high release probability. In addition, MLI–MLI synapses and MLI–Purkinje cell synapses are depressing, indicating a high release probability and relatively slow SV recruitment after release (Caillard et al., 2000; Pulido et al., 2015). Synaptic depression at MLI–Purkinje cell synapses depends on the presence of a high concentration of the slow endogenous calcium buffer parvalbumin (Caillard et al., 2000; Eggermann and Jonas, 2012). Parvalbumin is thought to favor depression by preventing calcium-dependent SV replenishment while keeping the exocytosis probability of docked SVs relatively unaffected (Caillard et al., 2000; Eggermann and Jonas, 2012). Overall, GABA release in MLI axons displays the features of high–release probability synapses. In agreement with this view we recently estimated the probability of docked SVs at MLI–MLI synapses at 0.84, a value close to 1 (Pulido et al., 2015). Such a high p value is a promising starting point when searching for a depressing/facilitating sequence. It is important to note, however, that we also found that the resting docking site occupancy, δ, was <1 (Pulido et al., 2015). Therefore, because δ was estimated at 0.51, the combined release probability per docking site was 0.51 × 0.84 = 0.43, markedly lower than p (Pulido et al., 2015; Eq. 6).

To induce a depression/facilitation sequence, we considered increasing the release probability even further by applying presynaptic depolarization. MLI axons are relatively short (~200 µm) and are electrically compact, so that subthreshold somatic depolarization is partially transmitted to presynaptic terminals (Glitsch and Marty, 1999; Mejia-Gervacio et al., 2007). This induces an elevation of the presynaptic calcium concentration and an enhancement of asynchronous transmitter release (Glitsch and Marty, 1999; Bouhours et al., 2011; Christie et al., 2011). Evoked synaptic currents are either increased or unchanged and display in all cases a reduced PPR (Bouhours et al., 2011; Christie et al., 2011). Recently, we analyzed this effect within the framework of the one-step model, finding that presynaptic depolarization induces a small but significant increase in p, no change of δ, and a marked reduction of r, indicating that the main target of presynaptic depolarization is vesicle replenishment (Pulido et al., 2015). In the two-step model, r is replaced by a set of three parameters: s, ρ, and r′ (Fig. 3 A). Therefore, we asked whether changes in any of the parameters s, ρ, and r′ of that model could account for the effects of presynaptic depolarization on vesicle replenishment. As a first step toward this goal, we characterized the responses to train stimulation at two frequencies, 25 and 50 Hz, as well as the changes induced in these responses by alterations of the presynaptic holding potential.

Experiments were performed on synaptically connected MLI–MLI pairs. As shown in Fig. 5 A, the postsynaptic holding potential was fixed at −60 mV, and the presynaptic holding potential was cyclically altered during periods of 9 s at −60, −50, and −80 mV. At the end of each 9-s period, a series of 5 voltage pulses (at 25 Hz) or 10 voltage pulses (at 50 Hz) was given to elicit APs in the axon, and the corresponding PSCs were recorded. Previous measurements indicate that membrane depolarization does not alter calcium entry (Bouhours et al., 2011). As shown in the exemplar traces of Fig. 5 B, using 25-Hz stimulation, presynaptic depolarization inhibited the responses for i = 2 and 3, whereas presynaptic hyperpolarization had the opposite effect. In the corresponding mean traces (Fig. 5 B, bottom), peak postsynaptic current amplitudes for i = 1 are similar at −60 and −50 mV and slightly reduced at −80 mV. In contrast, for i = 2, presynaptic depolarization and hyperpolarization respectively appear inhibitory and excitatory. This was confirmed by analyzing mean PSC amplitudes and corresponding ±SEM excursions as shown in Fig. 5 C. For i = 2, depolarizing the holding potential inhibited the responses (18.4 ± 6.6 and −50 mV vs. 60.6 ± 11.0 at −60 mV; $P < 0.002$), whereas hyperpolarizing the holding potential had a potentiating effect (104.3 ± 15.6 at −80 mV, $P < 0.02$, vs. −60 mV data). For i = 3, depolarizing the holding potential inhibited the responses (32.0 ± 10.0 at −50 mV vs. 81.4 ± 12.6 at −60 mV; $P < 0.002$), whereas hyperpolarizing the holding potential had no significant effect.

Group results are shown in Fig. 5 D. Two sets of experiments were performed, one at 25 Hz ($n = 12$) and another one at 50 Hz ($n = 8$). In both cases, the mean PSC amplitude for i = 1 was close to 200 pA and was not significantly dependent on presynaptic holding potential. Likewise, late in the train, for i = 4–5, there was no significant dependence of the PSC amplitude on the holding potential. For i = 2, however, PSC amplitudes were significantly lower at −50 mV than at −60 mV (16.4 ± 4.4 and 34.0 ± 8.5 at 25 Hz, $P < 0.05$, and 22.1 ± 7.9 and 36.8 ± 11.0 at 50 Hz, $P < 0.05$, respectively) and were likewise lower at −60 mV than at −80 mV (34.0 ± 8.5 and 57.4 ± 14.4 at 25 Hz, $P < 0.05$, and 36.8 ± 11.0 and 64.3 ± 17.4 at 50 Hz, $P < 0.05$, respectively). Likewise, for i = 3, PSC amplitudes were significantly lower at −50 mV than at −60 mV (25.5 ± 7.3 and 43.4 ± 11.9 at 25 Hz, $P < 0.05$, and 26.7 ± 8.1 and 61.6 ± 18.0 at 50 Hz, $P < 0.05$, respectively). These results indicate that depolarizing the holding potential strongly and significantly reduces PSC amplitudes for the second and third stimuli, leaving other responses close to their reference values. This selective inhibition results in a depression/facilitation sequence in the responses obtained at −50 mV (Fig. 5, C and D, orange curves).

Converting peak current data to docking site release probability for the study of short-term synaptic plasticity

To interpret the results of Fig. 5 in terms of the docking site models of Figs. 1 and 3, we need to transform PSC amplitude data into release probability data. A critical step in this analysis is to

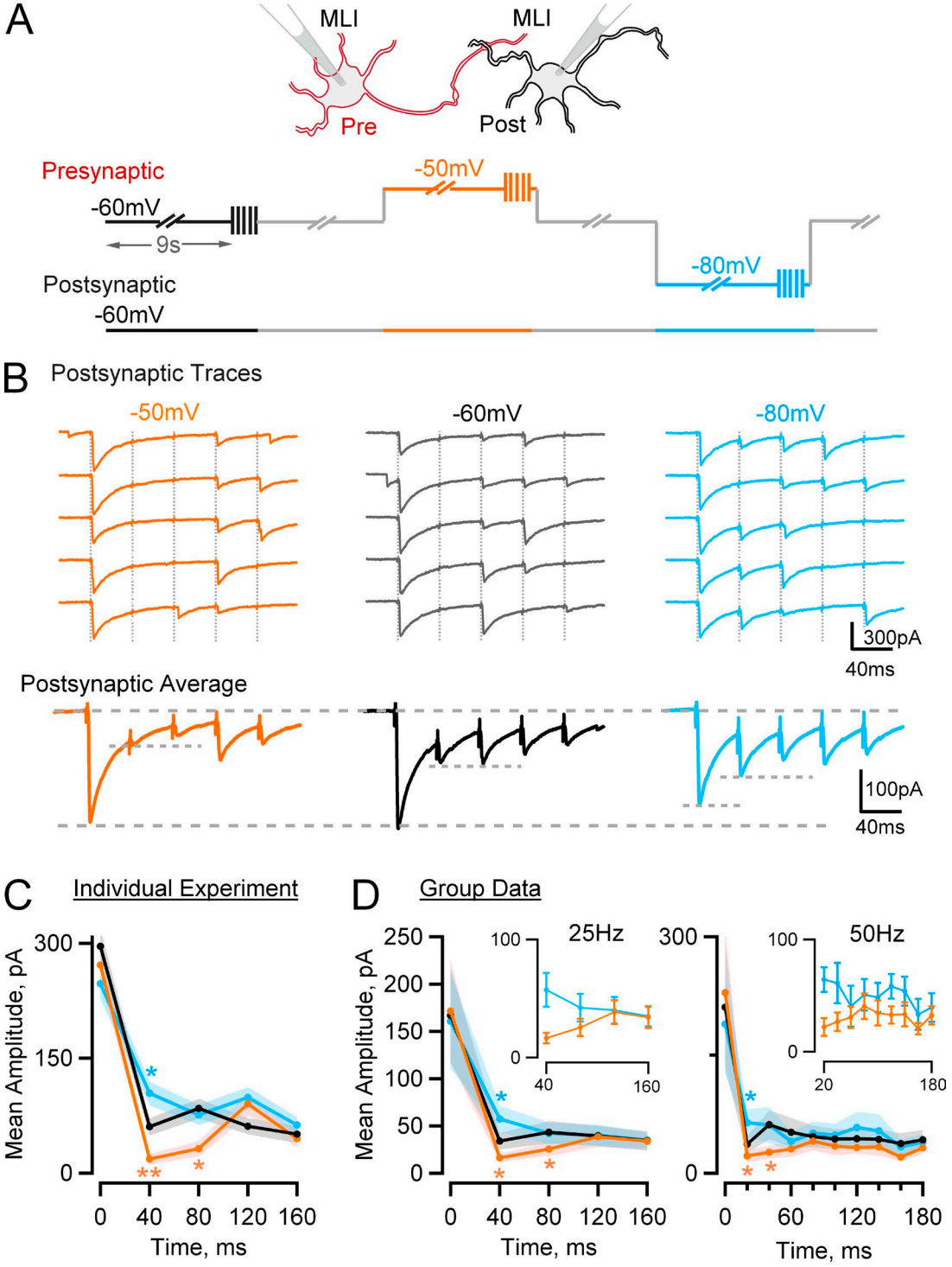

Figure 5. **Presynaptic holding potential changes alter the pattern of PSC amplitudes at MLI–MLI synapses during train stimulation. (A)** Scheme describing the experimental procedure. Synaptically connected MLIs were recorded under whole-cell configuration. The presynaptic cell was cyclically stimulated with a pattern given at −60 (black), −50 (red), or −80 mV (blue), consisting of a 9-s prepulse followed by a train of APs at 25 or 50 Hz, whereas the postsynaptic cell was kept at −60 mV. **(B and C)** Representative experiment from a presumed six–docking sites synapse. **(B)** Top: Consecutive postsynaptic responses to trains of presynaptic APs (25 Hz; timing indicated by vertical dotted gray lines) grouped according to the presynaptic holding potential. Bottom: Mean PSCs showing increased synaptic depression with depolarizing prepulse and decreased synaptic depression with hyperpolarizing prepulse. **(C)** Postsynaptic mean amplitudes as a function of stimulus time from the experiment shown in B. **(D)** Summary results from 12 synapses stimulated at 25 Hz (left) and 8 synapses stimulated at 50 Hz (right). Peak responses for different holding potentials are similar for i = 1 (first AP) and at the end of the train but differ for the second and third APs. (insets) Expanded view of PSC amplitudes starting from the second AP in the −50- (red) and −80-mV (blue) protocols. ±SEM intervals are indicated by shaded colored areas in C and D, main panels, and by error bars in D, insets. Note that individual entries represent trials from one experiment in C and means from various experiments in D. In C and D, statistically significant differences from the results at a holding potential of −60 mV are indicated as follows: *, $P < 0.05$; **, $P < 0.01$.

determine the total number of docking sites, N, participating in the recording. Knowing N is necessary to calculate p because the synaptic response scales with N. Provided that postsynaptic receptor saturation and synaptic jitter are limited, it is possible to determine N based on variance analysis of peak PSC amplitudes (Clements, 2003). Alternatively, if docking sites are independent and if N is reasonably small, an estimate may be obtained from an analysis of the pattern of failures during an AP train (Dobrunz and Stevens, 1997; Pulido et al., 2015). Compared with variance analysis, this approach has the advantage that it is less sensitive to errors linked to receptor saturation or synaptic jitter. Because the extent of receptor saturation is very significant at MLI–MLI synapses (Auger et al., 1998), this approach was preferred in the present work. The successive steps of the conversion from PSC amplitudes to release probabilities are illustrated in Fig. 6, whereas a detailed justification of the procedures can be found in Materials and methods, as well as in Pulido et al. (2015).

Docking site occupancy as a function of presynaptic holding potential and stimulus number

The first step of the analysis is presented in Fig. 6 (A and B). The raster plot of Fig. 6 A represents success/failure sequences for the experiment shown in Fig. 5 (B and C). In this plot, the probability of failures increases as a function of stimulus number, indicating synaptic depression. In addition, it may be seen that the probability of success for late stimulations gradually decreases as the holding potential is depolarized. This translates to a decrease with depolarization of the ratio of success for late events $P(S_{late})$ over the success probability for the first event $P(S_1)$ (Pulido et al., 2015; here, $P[S_{late}]$ is calculated for stimulation numbers 4–5 for 25-Hz trains and for stimulation numbers 5–10 for 50-Hz trains). From the group data of Fig. 6 B, this ratio decreased from 0.52 ± 0.04 at −80 mV holding potential to 0.36 ± 0.05 at −50 mV holding potential for 25-Hz stimulations ($P < 0.01$) and likewise from 0.37 ± 0.06 at −80 mV holding potential to 0.25 ± 0.04 at −50 mV holding potential for 50-Hz stimulations ($P < 0.005$). In addition, the holding potential changed the pattern of $P(S_i)$ values during a train, producing maximal effects for i = 2 and i = 3. At 25 Hz, for −50-mV depolarizations, the success rate was only 0.15 ± 0.03 for i = 2 and rebounded later to 0.27 ± 0.04 for i = 4–5 ($P < 0.02$). Likewise, at 50 Hz, the success rate was 0.085 ± 0.036 for i = 2 and rebounded later to 0.18 ± 0.04 for i = 5–10 ($P < 0.05$). Collectively, these results confirm the presynaptic nature of the depression/facilitation sequence obtained at depolarized holding potential. They indicate that the release probability, like the peak PSC amplitude, follows a depression/facilitation sequence after presynaptic depolarization.

Calculating release probabilities per docking site

The probabilities $P(S_i)$ shown in Fig. 6 B are related to individual synapses, as derived from paired recordings. Next, we transformed this information into probabilities per docking site, $P_D(S_i)$, for comparison with the models of Figs. 1 and 3. MLI–MLI synapses are called "simple" when they involve a single presynaptic active zone and a single postsynaptic density and are called "multiple" otherwise (Kondo and Marty, 1998; Pulido et al., 2015). From an analysis of the failure rate at resting holding potential, it is possible to estimate the number of docking sites present in one synapse (Pulido et al., 2015; Materials and methods). This analysis is valid independently of whether the synapse is simple or not, provided that docking sites are independent and have similar release properties. Therefore, in the present work, we mixed together results obtained from simple synapses (as exemplified in Fig. 7 of Pulido et al. [2015]) and multiple synapses (as exemplified in Fig. 5), calculating in each case the total number of participating docking sites. These numbers averaged 4.0 ± 0.9 at 25 Hz ($n = 12$, including 7 simple synapses and 5 multiple synapses) and 3.9 ± 1.0 at 50 Hz ($n = 8$, including 3 simple synapses and 5 multiple synapses). With the docking site numbers in hand, we followed our previous method to estimate the probability of release per docking site, $P_D(S_i)$, from the $P(S_i)$ results (Pulido et al., 2015). The $P_D(S_i)$ results showed essentially the same features as the $P(S_i)$ results from which they were derived, as may be seen by comparing Fig. 6 B with Fig. 6 C. The advantage of the $P_D(S_i)$ analysis is that it gives numbers that are directly relevant to underlying mechanisms of vesicular release, according to the equation $P_D(S_i) = p\,\delta_i$. We found at a holding potential of −50 mV that for 25-Hz stimulations, $P_D(S_1)$ averages 0.46 ± 0.08, whereas for stimulation 2, $P_D(S_2)$ drops to 0.053 ± 0.013. An even more dramatic decrease was found between stimulations 1 and 2 at 50 Hz with values $P_D(S_1) = 0.49 \pm 0.10$ and $P_D(S_2) = 0.022 \pm 0.008$, respectively. Later in the train, a clear rebound occurred, with steady-state values of $P_D(S_{4-5}) = 0.09 \pm 0.01$ at 25 Hz (larger than $P_D[S_2]$, $P < 0.05$) and $P_D(S_{5-10}) = 0.06 \pm 0.01$ at 50 Hz (larger than $P_D[S_2]$, $P < 0.01$). These results show that $P_D(S_i)$ curves exhibit a similar dependence on presynaptic potential as $P(S_i)$ curves.

Fig. 6 D illustrates PPR values calculated for individual docking sites ($PPR = P_D[S_2]/P_D[S_1]$), based on the results of Fig. 6 C. These values display a very marked dependence on holding potential. If we assume that the release probability of docked vesicles, p, is constant during a train, the PPR at the level of a single docking site can in view of Eq. 2 be written as $PPR = P_D(S_2)/P_D(S_1) = \delta_2/\delta$. Using the values of δ obtained by simulation (which are almost independent of the holding potential; see below), the effects of holding potential and stimulation frequency on δ_2 can be estimated (Fig. 6 D, bottom). At −50 mV, δ_2 is as low as 0.05 (25 Hz; about ninefold smaller than the initial docking site occupancy and 1.7-fold smaller than the steady state) or 0.02 (50 Hz; ∼22-fold smaller than the initial value and 2.7-fold smaller than the steady state). In summary, this analysis indicates a profound reduction of δ early in a train, particularly at −50 mV and at 50 Hz, and a substantial recovery later in the train.

Changes in presynaptic holding potential may be simulated within the two-step docking site model

Comparing the $P_D(S_i)$ curves in Fig. 6 C with the simulations of Fig. 1 shows that the one-step model is unable—at least in the simple version of Fig. 1; see below—to account for the depressing/facilitating sequence observed after presynaptic depolarization. In contrast, the results obtained with a −50-mV holding potential are strikingly similar to some of the simulations using the two-step model (e.g., Fig. 3 B, d, violet, blue, and cyan curves). Comparing the simulations of Fig. 3 B with the results of Fig. 6 C suggests that effects of presynaptic membrane potential may be

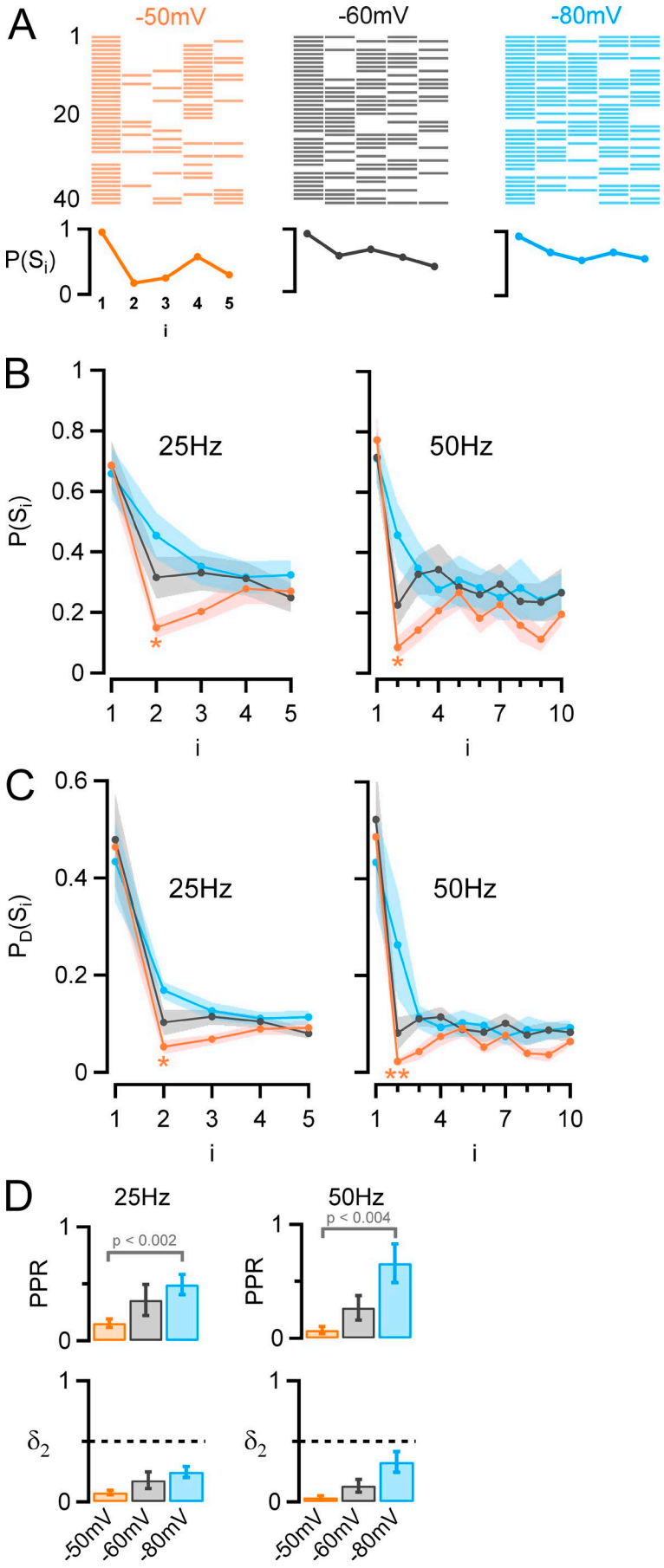
A
-50mV
-60mV
-80mV
1
20
40
P(Si)
1
0
1 2 3 4 5
i
B
25Hz
50Hz
P(Si)
1
0.8
0.6
0.4
0.2
0
1 2 3 4 5
1 4 7 10
i
C
25Hz
50Hz
PD(Si)
0.6
0.4
0.2
0
*
**
1 2 3 4 5
1 4 7 10
i
D
25Hz
50Hz
p < 0.002
p < 0.004
PPR
1
0
δ2
-50mV
-60mV
-80mV

largely explained by changes of ρ. However, the possibility was left open of changes of other parameters, particularly in view of our earlier finding that p slightly increases with depolarization (Pulido et al., 2015). Therefore, we performed complete simulations to obtain sets of parameters that would minimize the sum of least square deviations to mean data.

The results of these simulations are shown in Fig. 7. At a holding potential of −60 mV, and at 25-Hz stimulation frequency, optimal parameter values were δ = 0.5, p = 0.95, ρ = 0.65, r′ = 0.15, and s = 0.35 (Fig. 7 B, top; shaded area indicates mean ± SEM of group data, and dotted line indicates simulation). The two first parameter values are close to the values of 0.45 and 0.89 found earlier within the framework of the one-step model (Pulido et al., 2015). Keeping r′ and s values constant, simulations of $P_D(S_i)$ curves at a holding potential of −50 mV (Fig. 7 A, orange) and −80 mV (Fig. 7 C, blue) were obtained. Best fit values were δ = 0.45, p = 1.00, and ρ = 0.2 at −50 mV and δ = 0.5, p = 0.85, and ρ = 0.9 at −80 mV. These results confirm that effects of changing the presynaptic potential involve marked changes in ρ; by comparison, the contribution of p is modest, and that of δ is insignificant.

Fig. 7, bottom, shows the corresponding simulations for 50-Hz stimulation frequency. Parameter values for p, δ, and ρ were kept at the values found for 25-Hz simulations, but parameter values for r′ and s were adjusted to account for the change in interstimulus interval Δt. For parameter r′, we corrected the value according to the equation $r' = 1 - \exp(-R'\Delta t)$, assuming a constant value of R′. This gave r′ = 0.08 at 50 Hz, compared with r′ = 0.15 at 25 Hz. Applying a similar procedure for s (based on $s = 1 - \exp[-S\Delta t]$) yielded s = 0.20 at 50 Hz, compared with s = 0.35 at 25 Hz. These adjustments of r′ and s correctly predicted the dependence on frequency of the inhibition observed for i = 2 at −50 mV (Fig. 7 A, compare top and bottom). This led, however, to $P_D(S_i)$ simulations that were somewhat too low near steady state (Fig. 7, A–C, bottom, light color fits). A better fit was obtained by increasing r′ and s to 0.10 and to 0.24, respectively (Fig. 7 A–C, bottom, dark color fits). To justify these increases of r′ and s by 25% and 20%, we recall that docking site replenishment is Ca^{2+}-sensitive (Neher and Sakaba, 2008) and is therefore enhanced by AP-induced local Ca^{2+} concentration changes. Both the replacement site and the docking site are likely close to the site of Ca^{2+} entry, so that the local Ca^{2+} concentration near docked vesicles and replacement vesicles will be on average higher at 50-Hz stimulation than at 25-Hz stimulation. This will enhance the values of r′ and s at 50 Hz compared with the values derived from 25-Hz data for constant R′ and S.

These simulations show that effects of presynaptic depolarization can be mimicked by a combination of a small increase of p and of a strong decrease of ρ. At −50 mV, both the very high value of p and the small value of ρ contribute to deplete the docking site occupancy after the first stimulation, leading to a very low value of $P_D(S_2)$. Thereafter, the replacement site occupancy increases as new vesicles are recruited from the reserve pool, leading to an increase of docking site occupancy and to a rebound of the $P_D(S_i)$ response.

High release probability at MLI synapses

Our results and simulations indicate that p, the release probability of docked SVs, is very high. Because p is close to its maximal value of 1, changes in p as a function of holding potential are relatively small, with a 15% difference between −80- and −50-mV simulations (Fig. 7). Small changes in p are consistent with our previous finding that the amount of Ca^{2+} entry does not change significantly with the holding potential (Bouhours et al., 2011).

The two-step model, like the one-step model, predicts a limiting value PPR = 1 − p at high stimulation frequency (Eq. 8). According to this relation, large relative changes in the PPR can be achieved by modest increases in p, provided that p is close to 1. The steep relations of the PPR on potential shown in Fig. 6 D, top, observed at both 25- and 50-Hz stimulation rates, are therefore in line with the suggestions that p is close to 1 and that it increases with presynaptic depolarization. At the higher stimulation frequency of 50 Hz, the PPR reaches very low values at depolarized potentials (0.023 ± 0.013; Fig. 6 D, top right). Entering this value into Eq. 8 indicates that at −50 mV, p is >0.977. Accordingly, a parameter value p = 1 was chosen for the simulations of Fig. 7 A. Overall, the simulations highlight one of the reasons why the depressing/facilitating sequence only occurs in exceptional experimental conditions: this sequence requires a value of p that is very close to 1.

Can increased spontaneous release before stimulation explain the ρ decrease?

It has been shown that depolarization of the presynaptic holding potential in MLI axons leads to an increased rate of spontaneous SV release (Glitsch and Marty, 1999; Christie et al., 2011; Pulido et al., 2015). Can this effect account for the decrease in ρ that is apparent in our simulations? To address this question, we scaled with respect to N the total number of spontaneous PSCs observed in the 9-s pretrain period, finding a mean value per docking site of 4.53 ± 0.89 at −60 mV (n = 20). We found that this number was

Figure 6. **Effect of presynaptic holding potential on synaptic success rate and on docking site release probability. (A)** Top: Success (colored bars)/failure (white) sequences for a series of 40 consecutive trials. Bottom: Synaptic success probability as a function of i ($P[S_i]$), showing increased synaptic depression with depolarizing holding potential (red, −50 mV; black, −60 mV; blue, −80 mV; same experiment as in Fig. 5, B and C). **(B)** Group results (25 Hz, n = 12; 50 Hz, n = 8) showing that the success probability at i = 1 is not affected by prepulse holding potential; however, from i = 2, there is a decrease in success probability with presynaptic depolarization. This effect is strongest for i = 2 and i = 3. **(C)** Release probability per docking site ($P_D[S_i]$) as a function of i, showing, as in B, in depolarizing conditions a strong depression in response to the second AP followed by a rebound. **(D)** Top: PPR values derived from C as a function of holding potential, showing a strong reduction with depolarization (mean ± SEM, 25 Hz: 0.15 ± 0.04 at −50 mV, 0.36 ± 0.04 at −60 mV, 0.5 ± 0.09 at −80 mV; 50 Hz: 0.07 ± 0.03 at −50 mV, 0.27 ± 0.1 at −60 mV, 0.66 ± 0.17 at −80 mV). Bottom: Estimated docking site occupancy before the second stimulation as a function of holding potential (mean ± SEM, 25 Hz: 0.08 ± 0.02 at −50 mV, 0.18 ± 0.07 at −60 mV, 0.25 ± 0.04 at −80 mV; 50 Hz: 0.03 ± 0.01 at −50 mV, 0.13 ± 0.05 at −60 mV, 0.33 ± 0.08 at −80 mV). In B and C, statistically significant differences between the results for i = 2 and the results at steady state are indicated as follows: *, P < 0.05; **, P < 0.01.

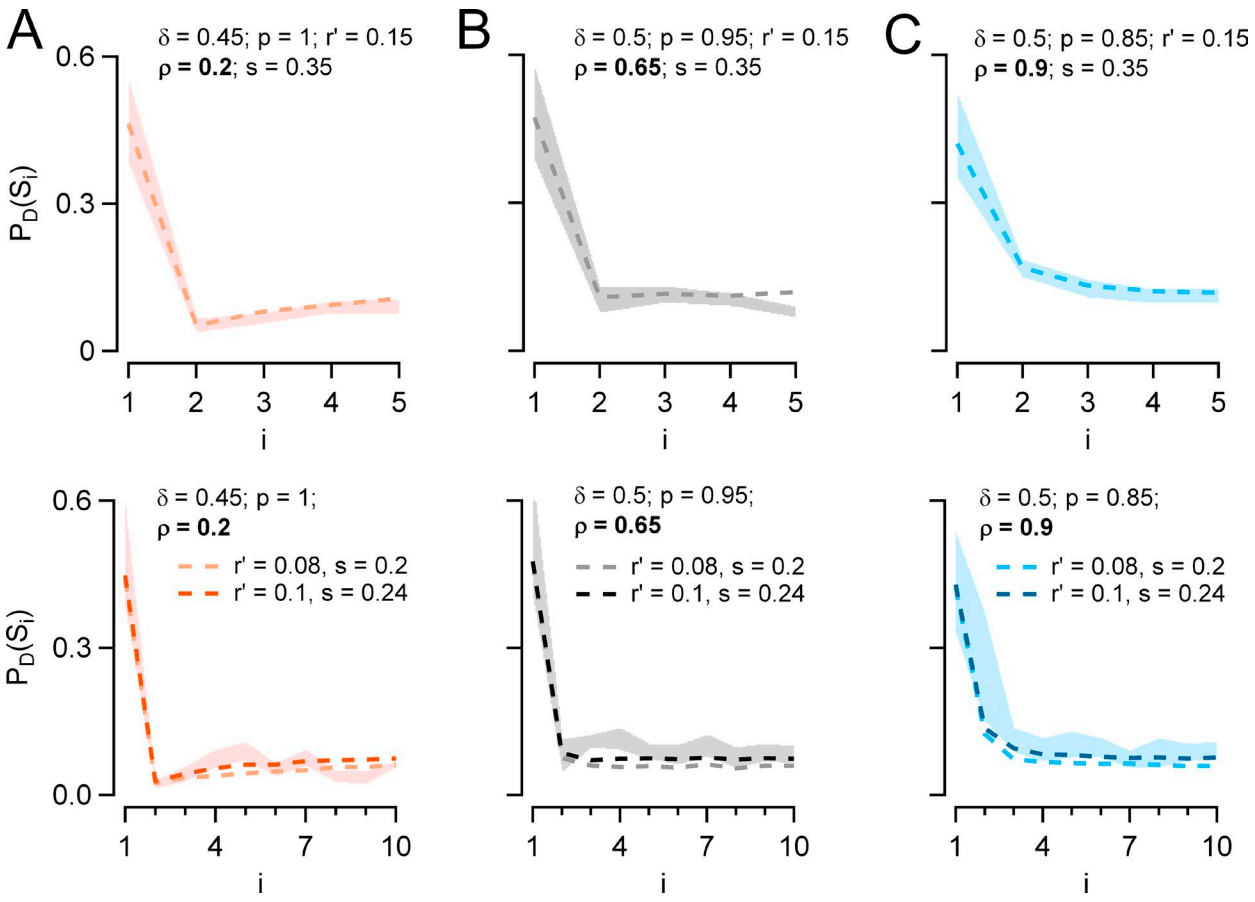

Figure 7. **Simulation of $P_D(S_i)$ plots with two-step release model. (A–C)** Plots of $P_D(S_i)$ as a function of i from Monte Carlo simulations performed at 25 (top) and 50 Hz (bottom) using the two-step model (dotted lines). Two parameters were fixed: r' and s. Two parameters changed with the presynaptic holding potential: at −50 mV, p = 1 and ρ = 0.2 (A, orange); at −60 mV, p = 0.95 and ρ = 0.65 (B, gray); and at −80 mV, p = 0.85 and ρ = 0.9 (C, blue). Finally, δ was taken at 0.45 at −50 mV and at 0.50 at both −60 and −80 mV. Corresponding experimental results are depicted by shaded areas (mean ± SEM; *n* = 12 pairs at 25 Hz and 8 pairs at 50 Hz). Both experimental data and simulations indicate the following: at −50 mV, a depression/facilitation sequence (A); at −60 mV, an abrupt fall between first and second stimulations followed by a flat $P_D(S_i)$ curve for i ≥ 2 (B); and at −80 mV, a monotonic depression (C). Top: At 25 Hz, the values of r' and s were r' = 0.15 and s = 0.35. Bottom: At 50 Hz, the values of r' and s were corrected for the change in frequency. This was done in two ways. In one variant, transition rates R' and S were the same as for the 25-Hz simulations, giving r' = 0.08 and s = 0.2 at 50 Hz (light-colored dashed lines). In the other variant, r' and s were increased to 0.1 and to 0.24, respectively, to take into account the increased speed of vesicle replenishment with calcium concentration (dark-colored dashed lines). δ, p, and ρ were as before. The second variant offers a slightly better fit than the first.

not different at −80 and −60 mV (−80 mV over −60 mV ratio: 0.99 ± 0.04, P = 0.8) but that it was significantly higher at −50 mV than at −60 mV (−50 mV over −60 mV ratio: 1.07 ± 0.03, P < 0.05). This indicates that in agreement with previous studies, somatic depolarization increases the rate of asynchronous release. When multiplied by the mean rate of 4.53 per docking site, the 7% increase at −50 mV corresponds to 0.32 additional release events per docking site. This difference is reasonably close to the difference in ρ values (0.65 − 0.20 = 0.45) obtained in the simulations of Fig. 7 between −60 and −50 mV. This indicates that the number of SVs lost because of increased spontaneous release is similar to the decrease in ρ revealed by the subsequent AP train. This in turn suggests that the increase in spontaneous release is offset by a loss of replacement SVs, whereas the stock of docked SVs remains roughly constant.

Other possible mechanisms

Our simulations suggest that the two-step model is compatible with our experimental results. However, alternative, more complicated models are not excluded. Data at the calyx of Held suggest that after exocytosis, docking sites are not immediately available, but that they need to be refurbished by a process that depends on endocytosis (Hosoi et al., 2009). This could give rise to a refractory period at each docking site after exocytosis (Neher, 2010). We found that incorporating such a refractory period into the one-step docking model can lead to a depression/facilitation sequence (Fig. 8). Under these conditions, we reconsidered whether we could account for the effects of depolarization with a single parameter change in the one-step model. Increasing either p (Fig. 8 A) or δ (Fig. 8 B) led to a depression/facilitation sequence. However, this sequence was accompanied by an increase in the responses to the first stimulation that was much stronger than experimentally observed. Increasing r to values near 0.5–0.6 also led to a depression/facilitating sequence (Fig. 8 C). However, the transition to the depression/facilitation pattern was accompanied by an increase in steady-state responses that contrasted with the decrease observed during presynaptic depolarization. Overall, no simple manipulation of the parameters in the one-step model

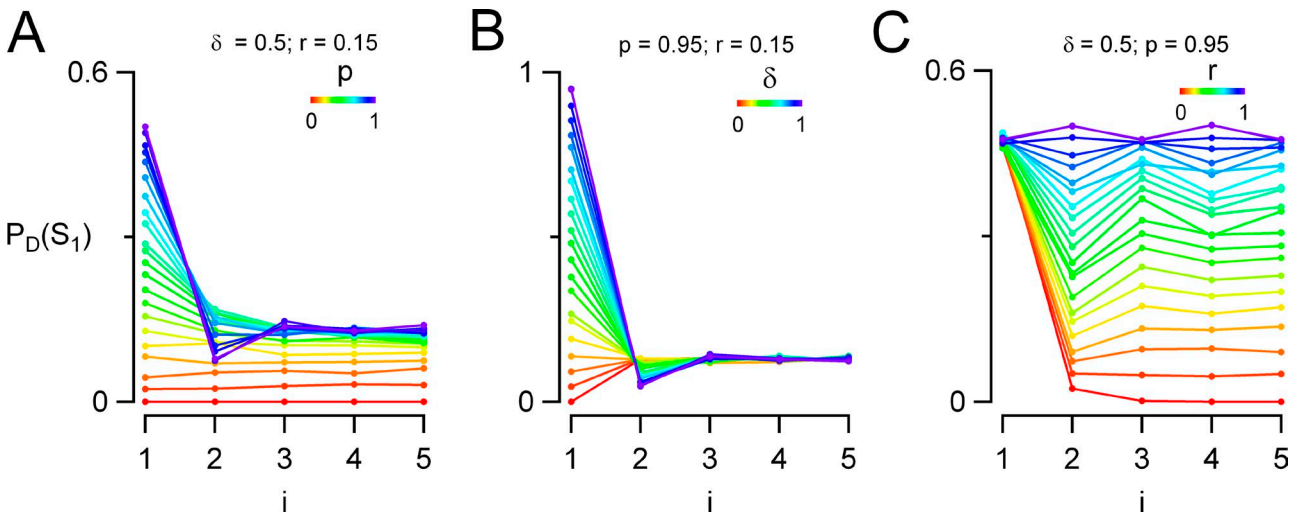

Figure 8. **Incorporating a refractory period in the one-step model.** In this variant of the one-step model, a refractory period was incorporated after each fusion event, preventing subsequent release at the same docking site during 40 ms. Simulations are as in Fig. 1 (25 Hz). Starting from the same reference values as in Fig. 1, parameters p (A), δ (B), and r (C) are separately increased in the range 0–1. For certain parameter combinations (dark blue curves in A and B and yellow/green curves in C), a depression/facilitation sequence occurs. However, all features of the depolarization experiments are not reproduced (see text).

could account for the effects of depolarization, even if a refractory period was included. Furthermore, the refractory period of Fig. 8 predicts a reduced release probability for the second trial if the first trial is a success, $P(S_2IS_1)$, compared with the value obtained if the first trial is a failure, $P(S_2IF_1)$. This effect should be particularly visible for elementary synapses comprising a single docking site (Pulido et al., 2015). Therefore, we reanalyzed our elementary synapse recordings to test for such an effect. However, we failed to detect any significant correlation between $P(S_2IF_1)$ and $P(S_2IS_1)$ values (0.120 ± 0.021 and 0.085 ± 0.029, respectively; P = 0.34, paired *t* test, $n = 11$). This analysis argues against a strong refractory period in MLI–MLI synapses and makes a participation of such a refractory period in the generation of the depression/facilitation sequence unlikely.

Another variant of the one-step model involves two release pathways operating in parallel. In various preparations including the calyx of Held (Neher and Sakaba, 2008), mossy fiber–granule cell synapses (Hallermann et al., 2010), and synapses between cartwheel cells and fusiform principal cells of the dorsal cochlear nucleus (Lu and Trussell, 2016), two sets of SVs are envisaged with different release probabilities. Because low-p SVs are consumed less rapidly than high-p SVs during a train, the relative contribution of low-p SVs to the overall response gradually increases, thus mitigating the effects of synaptic depression occurring for the high-p SVs (Neher, 2015; Lu and Trussell, 2016). Although in most cases the overall response displays a monotonic decrease (Hallermann et al., 2010; Neher, 2015; Lu and Trussell, 2016), if the two p values were widely different, the high-p pathway could be quickly depressing, whereas the low-p pathway would be slowly facilitating, potentially giving rise to a depression/facilitation sequence. Therefore, increasing the release probability of the high-release pathway could lead to a depression/facilitation sequence by accelerating the initial depression phase. In this case, a depression/facilitation sequence would occur for two sets of sites, each operating on the basis of the one-step model. Can this then be the case in our experiments? If this were the case, a fraction of docking sites would be facilitating, whereas the other fraction would be depressing. In our previous study of MLI–MLI synapses, we have encountered 11 cases of synapses containing a single docking site (elementary synapses). In all cases these synapses were depressing, and we have never encountered facilitating counterparts of these synapses (Pulido et al., 2015). This argues against a parallel model with different p values to explain the depression–facilitation sequence observed here.

Overall, variants of the one-step model could account for the depression/facilitation sequence in certain conditions. In the present preparation, however, the two-step model received independent support from a recent analysis of cumulative variance of release counts during trains (Miki et al., 2016). Hence, at MLI–MLI synapses, the two-step model is an attractive, parsimonious hypothesis that accounts both for statistical properties of SV release and for patterns of short-term synaptic plasticity.

Discussion

In the present work, we examine the predictions of two models of docking site occupancy (one-step model and two-step model) on short-term synaptic plasticity. We show that both one-step and two-step models can predict the behavior of depressing and of facilitating synapses without necessitating changes of the release probability p during a train. Furthermore, we show that the parameter space describing release probability, replenishment rate, and initial docking site occupancy can be partitioned in two regions corresponding to depressing and facilitating synapses. Next we show that whereas predicted synaptic responses are monotonic in the one-step model, the two-step model can predict facilitating/depressing sequences and depressing/facilitating sequences in addition to continuously facilitating or depressing sequences. As an illustration of this analysis in a specific form of synaptic plasticity, we finally show that at MLI–MLI synapses,

presynaptic depolarization induces a depression/facilitation sequence during train stimulations. This unusual form of short-term synaptic plasticity is inconsistent with the one-step model but is readily explained by the two-step model. Within the two-step model, the depression/facilitation sequence results from a reduced probability of occupancy of the replacement site after presynaptic depolarization, together with a small increase in the release probability of docked SVs.

Changes in docking site occupancy explain changes in synaptic strength during AP trains

Our simulations (Figs. 1 and 3) illustrate a surprisingly wide variety of response patterns in response to AP trains, including facilitating, depressing, facilitating/depressing, and depressing/facilitating sequences. These differences are based exclusively on changes of δ after recent synaptic activity. Additional effects such as changes of p during a train remain possible but are not taken into consideration here for the sake of simplicity.

The simulations provide a portfolio of changes in synaptic strength patterns during AP trains in response to modifications of individual parameters of either the one-step model (Fig. 1) or the two-step model (Fig. 3). Within the one-step model, changing p, δ, or r produces marked changes in the PPR (Fig. 1 C), and in each case, the relation between PPR and initial docking site release probability ($P_D[S_1]$) takes a specific shape (Fig. 1 D). In the two-step model, changing any of the parameters p, δ, r′, ρ, or s not only changes the PPR (Fig. 3 C) but can also produce non-monotonic $P_D(S_i)$ plots, including patterns showing a depression/facilitation sequence (Fig. 3 B). Based on this analysis, comparing experimental $P_D(S_i)$ plots with the various simulations of Figs. 1 B and 3 B provides a way to identify candidate parameter(s) that could be changed during a specific synaptic modification. This parameter identification is a potentially powerful tool to identify underlying cellular or molecular changes.

Facilitating versus depressing synapses

A key feature of our simulations, in accordance with our previous work at MLI–MLI synapses, is that the value of δ is <1 at rest (Trigo et al., 2012; Pulido et al., 2015). This contrasts with the traditional assumption that δ = 1. The proposal that δ < 1 at rest is consistent with recent electron microscopy data indicating incomplete or reversible docking of SVs under certain conditions (Imig et al., 2014; He et al., 2017; Chang et al., 2018). At the beginning of an AP train, exocytosis is elicited by APs, leading to docking site depletion. However, at the same time, docking site replenishment is activated by the presynaptic calcium elevation resulting from cumulated calcium entry (Neher and Sakaba, 2008). Therefore, provided that the initial value of δ is <1, facilitation occurs if docking site replenishment is faster than exocytosis of docked SVs (Miki et al., 2016). Specifically, by rearranging Eq. 5, it appears that facilitation (PPR > 1) occurs if the probability of replenishment verifies the condition $r > p/(p + 1/\delta - 1)$. When considering this inequality, it may be noted that if δ = 1, the condition becomes r > 1, which is impossible to fulfill because r is a probability and cannot exceed the value of 1. This explains the inability of docking site models to account for facilitation when assuming that δ = 1. On the other hand, if δ < 1, the above inequality implies that in agreement with Fig. 2, any depressing synapse can be made facilitating by either decreasing p or increasing r.

PPR, release probability, and docking site occupancy

It has long been recognized that at depressing synapses, the PPR recorded at short interstimulus intervals depends linearly on release probability, following the simple equation PPR = 1 − p (Betz, 1970; Rozov et al., 2001; Lu and Trussell, 2016; Eq. 8). It is important to reflect on the meaning of p in this equation. Because δ < 1, p differs from the initial release probability per docking site $P_D(S_1)$, according to the relation $P_D(S_1) = \delta p$ (Eq. 6). Because $P_D(S_1)$ is proportional to the synaptic strength, the directly accessible relation from an experimental point of view is that between PPR and $P_D(S_1)$. As shown in Fig. 1 C, a, and Fig. 3 C, a, both the one-step model and the two-step model conform to the prediction that PPR = 1 − p at small interstimulus intervals. The resulting relation between PPR and $P_D(S_1)$ is also linear, but now the slope is 1/δ (because combining Eqs. 6 and 8 yields $PPR = 1 - P_D[S_1]/\delta$), not 1, as illustrated in Fig. 1 D for the one-step model. Thus, if p is responsible for changing the synaptic strength, the slope of the PPR versus $P_D(S_1)$ curve provides a direct way to calculate δ.

Another consequence of the finding that δ is not fixed at a value of 1 is that δ is a possible target for modulation of synaptic strength, alternative to p. In contrast to the linear relation between PPR and p, the relation between PPR and δ is hyperbolic for both one-step and two-step models, as illustrated in Fig. 1 C, b, and Fig. 3 C, b. This leads to hyperbolic relations between PPR and $P_D(S_1)$ for the case that δ is responsible for synaptic changes, as shown in Fig. 1 D, b, for the case of the one-step model. The different shapes of the PPR versus $P_D(S_1)$ curves depending on the mechanism underlying changes in synaptic strength (linear for changes in p and hyperbolic for changes in δ) provide a useful tool to distinguish between changes in p and changes in δ.

The depression/facilitation sequence induced by presynaptic depolarization at MLI–MLI synapses indicates a two-step rather than a one-step docking model

Results obtained at MLI–MLI synapses when applying long presynaptic depolarization are at first sight paradoxical because they indicate a small change in $P_D(S_1)$ together with a strong decrease of the PPR (Bouhours et al., 2011; Christie et al., 2011). In the framework of the one-step model, such a pattern resembles the situation where r is decreased (Fig. 1 D, c). However, the one-step model fails to explain the depression/facilitation sequence observed in Figs. 5 and 6 after presynaptic depolarization. Therefore, the finding that the two-step model accounts for this sequence (Fig. 7, left) gives support for the two-step model at this synapse. This conclusion is in line with results obtained with variance–mean analysis of simple MLI–MLI synapses (Miki et al., 2016).

Respective contributions of p increase and ρ decrease during depolarization-induced depression/facilitation sequence

As shown in Fig. 3 B, the depression/facilitation sequence is favored by high p values (Fig. 3 B, a) and by low ρ values (Fig. 3 B, d). When both conditions are fulfilled, δ strongly decreases after

the first stimulation and is then partially restored because of gradual SV recruitment from the replacement site, thus creating the characteristic depression/facilitation sequence observed after depolarization.

Changes in $P_D(S_i)$ plots versus presynaptic holding potential at MLI–MLI synapses (Fig. 5 C) are close to the pattern expected from ρ changes (Fig. 3 B, d) but differ from that expected from p changes (Fig. 3 B, a). Both parameter changes actually contribute, albeit to different degrees. Previous results have indicated an increase in release probability caused by an increase in either Ca^{2+} entry (Christie et al., 2011) or PKC activity (Bouhours et al., 2011) and a decrease in replenishment rate (Pulido et al., 2015). The stronger contribution of ρ changes within the two-step model is consistent with the earlier finding by Pulido et al. (2015) of a strong contribution of r within the one-step model. On the other hand, p changes are limited by the fact that p is close to its maximum of 1 under control conditions (Pulido et al., 2015).

Mechanism of replacement site depletion

We find a numerical correspondence between the increase in spontaneous SV release during predepolarization and the subsequent depletion of the replacement site, suggesting a causal link between the two phenomena. However, a rigorous test of this suggestion would require the knowledge of numerical values for the rate constants S and R′ before AP trains. It is well established that SV replenishment is sensitive to the cytosolic Ca^{2+} concentration (Neher and Sakaba, 2008), so that it is expected that either or both S and R′ should take lower values before the AP train than those apparent in our simulations, but at present, putting any number on these values would be premature. As p increases because of depolarization, R′ probably also increases such that δ is maintained near its control value in spite of spontaneous release. However, S probably does not increase in the same proportion such that the replacement site is not replenished, leading to a drop of ρ. This mechanism likely limits spontaneous release in the long run during depolarization and thus spares the resources of the synapse, whereas the conservation of normal δ value ensures a normal response to a subsequent AP stimulation.

Possible reasons for the scarcity of reported examples of depression/facilitation sequence

Our results and analysis suggest that the depression/facilitation sequence results from a combination of high p and low ρ values. The first condition fits with the observation that at the neuromuscular junction, the depression/facilitation sequence is favored by elevating the external Ca^{2+} concentration and by applying posttetanic potentiation (Elmqvist and Quastel, 1965). It is also in line with the notion that the quick initial depression necessary for depression/facilitation sequence requires a high p value. The condition $\rho < 1$ is more novel and is worth considering in some detail. This condition expresses the fact that a late rise of δ after extensive initial release can only come from an increase in ρ. To provide insight into the relations between δ and ρ, it may be noted that making $p = 1$ in Eq. 3 leads to $\delta_{i+1} = r$. This indicates that for high p values, any δ rise must come from r. However, as shown in Eq. 9, r_i (the variant of r in the two-step model) is a linear function of ρ_i. It follows from these arguments that a growth of r_i as a function of i can only come from a growth of ρ_i as a function of i; this in turn is only possible if $\rho < 1$. Therefore, just like the starting condition $\delta = 1$ forbids facilitation, the starting condition $\rho = 1$ forbids the depression/facilitation sequence.

To explain the scarcity of experimental examples of the depression/facilitation sequence, it is tempting to speculate that the resting value of ρ is high in most synapses. In line with this suggestion, our simulations suggest a high resting ρ value in MLI–MLI synapses; only because of the transient ρ reduction induced by prolonged presynaptic depolarization does the depression/facilitation sequence become possible. One possible mechanism leading to a high resting ρ value in most synapses would be if the transition from replacement site to docking site were reversible with a high backward rate.

Applicability of two-step model of synaptic plasticity across mammalian central synapses

The present work shows that the two-step model offers a flexible and parsimonious framework to interpret a variety of time profiles of synaptic responses. It is still unclear to what extent this model applies across central mammalian synapses. Parallel fiber–Purkinje cell synapses, taken by Dittman et al. (2000) as illustrating facilitating synapses (or low-p synapses), have recently been shown to follow a variant of the two-step model (Doussau et al., 2017). Our work suggests that MLI–MLI synapses, representative of depressing synapses (a category represented by the climbing fiber–Purkinje synapses in the classification of Dittman et al. [2000]), as well as PF–MLI synapses, taken by Dittman et al. (2000) as representing mixed (facilitating–depressing) synapses, both follow the two-step model (Miki et al., 2016; this study). Therefore, of the three broad categories of synapses proposed by Dittman et al. (2000), all have been shown to conform at least in part with the two-step model. This raises the possibility that the two-step model could be broadly relevant to explain short-term synaptic plasticity in mammalian central synapses.

Acknowledgments

This work was supported by an H2020 European Research Council Advanced Grant (SingleSite, 294509) to A. Marty.

The authors declare no competing financial interests.

Author contributions: C. Pulido and A. Marty designed experiments, interpreted the results, and wrote the manuscript. C. Pulido carried out experiments and simulations.

José D. Faraldo-Gómez served as editor.

Submitted: 21 March 2018
Accepted: 23 May 2018

References

Arai, I., and P. Jonas. 2014. Nanodomain coupling explains Ca^{2+} independence of transmitter release time course at a fast central synapse. *eLife.* 3:e04057. https://doi.org/10.7554/eLife.04057

Auger, C., S. Kondo, and A. Marty. 1998. Multivesicular release at single functional synaptic sites in cerebellar stellate and basket cells. *J. Neurosci.* 18:4532–4547. https://doi.org/10.1523/JNEUROSCI.18-12-04532.1998

Bao, J., K. Reim, and T. Sakaba. 2010. Target-dependent feedforward inhibition mediated by short-term synaptic plasticity in the cerebellum. *J. Neurosci.* 30:8171–8179. https://doi.org/10.1523/JNEUROSCI.0276-10.2010

Betz, W.J. 1970. Depression of transmitter release at the neuromuscular junction of the frog. *J. Physiol.* 206:629–644. https://doi.org/10.1113/jphysiol.1970.sp009034

Bouhours, B., F.F. Trigo, and A. Marty. 2011. Somatic depolarization enhances GABA release in cerebellar interneurons via a calcium/protein kinase C pathway. *J. Neurosci.* 31:5804–5815. https://doi.org/10.1523/JNEUROSCI.5127-10.2011

Caillard, O., H. Moreno, B. Schwaller, I. Llano, M.R. Celio, and A. Marty. 2000. Role of the calcium-binding protein parvalbumin in short-term synaptic plasticity. *Proc. Natl. Acad. Sci. USA.* 97:13372–13377. https://doi.org/10.1073/pnas.230362997

Chang, S., T. Trimbuch, and C. Rosenmund. 2018. Synaptotagmin-1 drives synchronous Ca^{2+}-triggered fusion by C_2B-domain-mediated synaptic-vesicle-membrane attachment. *Nat. Neurosci.* 21:33–40. https://doi.org/10.1038/s41593-017-0037-5

Charlton, M.P., S.J. Smith, and R.S. Zucker. 1982. Role of presynaptic calcium ions and channels in synaptic facilitation and depression at the squid giant synapse. *J. Physiol.* 323:173–193. https://doi.org/10.1113/jphysiol.1982.sp014067

Christie, J.M., D.N. Chiu, and C.E. Jahr. 2011. Ca(2+)-dependent enhancement of release by subthreshold somatic depolarization. *Nat. Neurosci.* 14:62–68. https://doi.org/10.1038/nn.2718

Clements, J.D. 2003. Variance-mean analysis: A simple and reliable approach for investigating synaptic transmission and modulation. *J. Neurosci. Methods.* 130:115–125. https://doi.org/10.1016/j.jneumeth.2003.09.019

Del Castillo, J., and B. Katz. 1954. Statistical factors involved in neuromuscular facilitation and depression. *J. Physiol.* 124:574–585. https://doi.org/10.1113/jphysiol.1954.sp005130

Dittman, J.S., A.C. Kreitzer, and W.G. Regehr. 2000. Interplay between facilitation, depression, and residual calcium at three presynaptic terminals. *J. Neurosci.* 20:1374–1385. https://doi.org/10.1523/JNEUROSCI.20-04-01374.2000

Dobrunz, L.E., and C.F. Stevens. 1997. Heterogeneity of release probability, facilitation, and depletion at central synapses. *Neuron.* 18:995–1008. https://doi.org/10.1016/S0896-6273(00)80338-4

Doussau, F., H. Schmidt, K. Dorgans, A.M. Valera, B. Poulain, and P. Isope. 2017. Frequency-dependent mobilization of heterogeneous pools of synaptic vesicles shapes presynaptic plasticity. *eLife.* 6:e28935. https://doi.org/10.7554/eLife.28935

Eggermann, E., and P. Jonas. 2012. How the 'slow' Ca^{2+} buffer parvalbumin affects transmitter release in nanodomain-coupling regimes. *Nat. Neurosci.* 15:20–22. https://doi.org/10.1038/nn.3002

Elmqvist, D., and D.M. Quastel. 1965. A quantitative study of end-plate potentials in isolated human muscle. *J. Physiol.* 178:505–529. https://doi.org/10.1113/jphysiol.1965.sp007639

Glitsch, M., and A. Marty. 1999. Presynaptic effects of NMDA in cerebellar Purkinje cells and interneurons. *J. Neurosci.* 19:511–519. https://doi.org/10.1523/JNEUROSCI.19-02-00511.1999

Hallermann, S., A. Fejtova, H. Schmidt, A. Weyhersmüller, R.A. Silver, E.D. Gundelfinger, and J. Eilers. 2010. Bassoon speeds vesicle reloading at a central excitatory synapse. *Neuron.* 68:710–723. https://doi.org/10.1016/j.neuron.2010.10.026

He, E., K. Wierda, R. van Westen, J.H. Broeke, R.F. Toonen, L.N. Cornelisse, and M. Verhage. 2017. Munc13-1 and Munc18-1 together prevent NSF-dependent de-priming of synaptic vesicles. *Nat. Commun.* 8:15915. https://doi.org/10.1038/ncomms15915

Hosoi, N., M. Holt, and T. Sakaba. 2009. Calcium dependence of exo- and endocytotic coupling at a glutamatergic synapse. *Neuron.* 63:216–229. https://doi.org/10.1016/j.neuron.2009.06.010

Imig, C., S.-W. Min, S. Krinner, M. Arancillo, C. Rosenmund, T.C. Südhof, J. Rhee, N. Brose, and B.H. Cooper. 2014. The morphological and molecular nature of synaptic vesicle priming at presynaptic active zones. *Neuron.* 84:416–431. https://doi.org/10.1016/j.neuron.2014.10.009

Ishiyama, S., H. Schmidt, B.H. Cooper, N. Brose, and J. Eilers. 2014. Munc13-3 superprimes synaptic vesicles at granule cell-to-basket cell synapses in the mouse cerebellum. *J. Neurosci.* 34:14687–14696. https://doi.org/10.1523/JNEUROSCI.2060-14.2014

Katz, B. 1969. The release of neural transmitter substances. Liverpool University Press, Liverpool. 60 pp.

Kondo, S., and A. Marty. 1998. Synaptic currents at individual connections among stellate cells in rat cerebellar slices. *J. Physiol.* 509:221–232. https://doi.org/10.1111/j.1469-7793.1998.221bo.x

Lee, J.S., W.-K. Ho, and S.-H. Lee. 2012. Actin-dependent rapid recruitment of reluctant synaptic vesicles into a fast-releasing vesicle pool. *Proc. Natl. Acad. Sci. USA.* 109:E765–E774. https://doi.org/10.1073/pnas.1114072109

Llano, I., and H.M. Gerschenfeld. 1993. Inhibitory synaptic currents in stellate cells of rat cerebellar slices. *J. Physiol.* 468:177–200. https://doi.org/10.1113/jphysiol.1993.sp019766

Lu, H.-W., and L.O. Trussell. 2016. Spontaneous activity defines effective convergence ratios in an inhibitory circuit. *J. Neurosci.* 36:3268–3280. https://doi.org/10.1523/JNEUROSCI.3499-15.2016

Mejia-Gervacio, S., T. Collin, C. Pouzat, Y.P. Tan, I. Llano, and A. Marty. 2007. Axonal speeding: Shaping synaptic potentials in small neurons by the axonal membrane compartment. *Neuron.* 53:843–855. https://doi.org/10.1016/j.neuron.2007.02.023

Miki, T., G. Malagon, C. Pulido, I. Llano, E. Neher, and A. Marty. 2016. Actin- and myosin-dependent vesicle loading of presynaptic docking sites prior to exocytosis. *Neuron.* 91:808–823. https://doi.org/10.1016/j.neuron.2016.07.033

Neher, E. 2010. What is rate-limiting during sustained synaptic activity: Vesicle supply or the availability of release sites. *Front. Synaptic Neurosci.* 2:144. https://doi.org/10.3389/fnsyn.2010.00144

Neher, E. 2015. Merits and limitations of vesicle pool models in view of heterogeneous populations of synaptic vesicles. *Neuron.* 87:1131–1142. https://doi.org/10.1016/j.neuron.2015.08.038

Neher, E. 2017. Some subtle lessons from the calyx of Held synapse. *Biophys. J.* 112:215–223. https://doi.org/10.1016/j.bpj.2016.12.017

Neher, E., and T. Sakaba. 2008. Multiple roles of calcium ions in the regulation of neurotransmitter release. *Neuron.* 59:861–872. https://doi.org/10.1016/j.neuron.2008.08.019

Pan, B., and R.S. Zucker. 2009. A general model of synaptic transmission and short-term plasticity. *Neuron.* 62:539–554. https://doi.org/10.1016/j.neuron.2009.03.025

Pouzat, C., and A. Marty. 1999. Somatic recording of GABAergic autoreceptor current in cerebellar stellate and basket cells. *J. Neurosci.* 19:1675–1690. https://doi.org/10.1523/JNEUROSCI.19-05-01675.1999

Pulido, C., and A. Marty. 2017. Quantal fluctuations in central mammalian synapses: Functional role of vesicular docking sites. *Physiol. Rev.* 97:1403–1430. https://doi.org/10.1152/physrev.00032.2016

Pulido, C., F.F. Trigo, I. Llano, and A. Marty. 2015. Vesicular release statistics and unitary postsynaptic current at single GABAergic synapses. *Neuron.* 85:159–172. https://doi.org/10.1016/j.neuron.2014.12.006

Quastel, D.M. 1997. The binomial model in fluctuation analysis of quantal neurotransmitter release. *Biophys. J.* 72:728–753. https://doi.org/10.1016/S0006-3495(97)78709-5

Rozov, A., N. Burnashev, B. Sakmann, and E. Neher. 2001. Transmitter release modulation by intracellular Ca^{2+} buffers in facilitating and depressing nerve terminals of pyramidal cells in layer 2/3 of the rat neocortex indicates a target cell-specific difference in presynaptic calcium dynamics. *J. Physiol.* 531:807–826. https://doi.org/10.1111/j.1469-7793.2001.0807h.x

Sakaba, T. 2006. Roles of the fast-releasing and the slowly releasing vesicles in synaptic transmission at the calyx of Held. *J. Neurosci.* 26:5863–5871. https://doi.org/10.1523/JNEUROSCI.0182-06.2006

Scheuss, V., and E. Neher. 2001. Estimating synaptic parameters from mean, variance, and covariance in trains of synaptic responses. *Biophys. J.* 81:1970–1989. https://doi.org/10.1016/S0006-3495(01)75848-1

Südhof, T.C. 2012. The presynaptic active zone. *Neuron.* 75:11–25. https://doi.org/10.1016/j.neuron.2012.06.012

Taschenberger, H., V. Scheuss, and E. Neher. 2005. Release kinetics, quantal parameters and their modulation during short-term depression at a developing synapse in the rat CNS. *J. Physiol.* 568:513–537. https://doi.org/10.1113/jphysiol.2005.093468

Taschenberger, H., A. Woehler, and E. Neher. 2016. Superpriming of synaptic vesicles as a common basis for intersynapse variability and modulation of synaptic strength. *Proc. Natl. Acad. Sci. USA.* 113:E4548–E4557. https://doi.org/10.1073/pnas.1606383113

Trigo, F.F., T. Sakaba, D. Ogden, and A. Marty. 2012. Readily releasable pool of synaptic vesicles measured at single synaptic contacts. *Proc. Natl. Acad. Sci. USA.* 109:18138–18143. https://doi.org/10.1073/pnas.1209798109

Zucker, R.S., and W.G. Regehr. 2002. Short-term synaptic plasticity. *Annu. Rev. Physiol.* 64:355–405. https://doi.org/10.1146/annurev.physiol.64.092501.114547